

Superconducting Phases of Calcium Intercalated Bilayer Graphene

Rouhollah Gholami

Physics Department, Faculty of Science Razi University, Kermanshah, Iran
Physics Department, Faculty of Science Ilam University, Ilam, Iran

Rostam Moradian*

Physics Department, Faculty of Science Razi University, Kermanshah, Iran
Nanoscience and Nanotechnology Research Center, Razi University, Kermanshah, Iran

Sina Moradian

Department of Electrical and Computer Engineering,
University of Central Florida, Orlando FL, USA

Warren E. Pickett

Department of Physics UC Davis, One Shields Avenue, Davis CA 95616, USA
(Dated: April 8, 2019)

Built on a realistic multiband tight binding model, mirror symmetry is used to map a calcium-intercalated bilayer graphene Hamiltonian onto two independent single layer graphene effective Hamiltonians with renormalized hopping integrals. To obtain tight binding parameters, each effective monolayer graphene Schrödinger equation is solved analytically and fitted to first principles band structure results. Treatment of the pairing Hamiltonian leads to two decoupled gap equations for each of these effective graphene monolayer sectors. The decoupled gap equations are solved analytically to obtain the order parameters for superconducting phases. Two “flat bands” crossing the Fermi energy, each related to the graphene-like structures, are responsible for two distinct superconductivity gaps that emerge. Depending on how much these bands are affected by the intercalant and which is closer to the Fermi energy, distorted s -wave or d -wave superconductivity may become dominant. Numerical calculations reveal that d -wave superconductivity is dominant in both sectors. Adopting the two gap viewpoint of superconductivity in C_6CaC_6 , the dominant d -wave states should have the same critical temperature. For these two dominant phases we present the relation of the pairing potential to the superconducting critical temperature T_c . Around $T_c = 2K$ these two relations intersect, similar to what has been observed experimentally.

I. INTRODUCTION

Discovery of new superconducting phases, often at low temperature, has been one of the active achievements in recent decades, sometimes overshadowed by the high profile effort to push toward higher temperature superconductors. Remarkable progress in the synthesis or fabrication of nanostructures in the recent years is opening new horizons in engineering the physical properties of new classes of materials.

Two dimensional phases, including superconducting ones,¹ received renewed attention from the discovery that monolayer graphene can be peeled off, and subsequently found that it can be synthesized from the gas phase. Graphite intercalation compound (GIC) superconductors have been known and studied for decades.² Pristine graphene does not host superconductivity due to the vanishing density of states (DOS) at the Dirac point. Graphene with unique band structure and vanishing effective carrier mass at the Dirac (charge neutrality) points has become of rising interest. Recent discovery of unconventional superconductivity in twisted bilayer graphene³ may realize a new class of superconductor. Beside this progress, superconductivity reported in Ca-intercalated bilayer graphene represents the thinnest limit of graphite intercalation compounds (GICs), at 4K⁴ and around 6.4K in Ca-doped graphene laminates⁵. Experimental evidence for superconductivity around 6K was reported in lithium decorated graphene⁶ and at 7.4K in few layer graphene by Li intercalation.⁷

Using *ab initio* anisotropic Migdal-Eliashberg theory including Coulomb interaction, Margine *et al.*⁸ concluded that C_6CaC_6 should support phonon mediated superconductivity with a critical temperature $T_c = 6 - 7K$, within the range of observations, and it exhibits two distinct superconducting gaps on the electron and hole Fermi surface pockets. Mathematically one can use symmetry properties of Bloch coefficients of AA and AB stacked bilayer graphene and interpret their Hamiltonian as two independent single layer pseudo-graphene structures.

In this manuscript we will take advantage of the observation that AA bilayer graphene mathematically reduces to two independent monolayer graphene-like systems. It will be shown that the question of superconducting phases in Ca-intercalated bilayer graphene C_6CaC_6 can be decoupled to two independent gap equations which can be solved analytically (or nearly so) to obtain pairing phases and the dependence of T_c on the pairing strength. Section

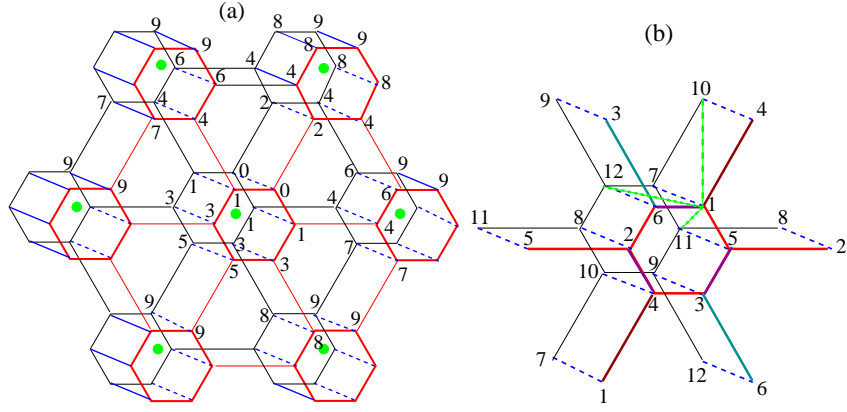


FIG. 1: Structure and notation. (a) Sketch (exaggerated) of shrunk bilayer graphene where numbers indicate C-C first, second, and so on, neighbors of reference carbon atom in each layer. (b) Intra-plane superconductor pairing amplitudes ($\Sigma_1 \Sigma_2 \Sigma_3$) are between 1-4, 3-6 and 2-5 subsites respectively, ($\Delta_1 \Delta_2 \Delta_3$) are between 3-5, 2-4 and 1-6 subsites respectively, and ($\Pi_1 \Pi_2 \Pi_3$) are between 2-6, 1-5 and 3-4 subsites respectively. Also, inter-plane superconductor pairing amplitudes ($\Sigma'_1 \Sigma'_2 \Sigma'_3$) are between 1-10, 3-12 and 2-11 subsites respectively, ($\Delta'_1 \Delta'_2 \Delta'_3$) are between 3-11, 2-10 and 1-12 subsites respectively, and ($\Pi'_1 \Pi'_2 \Pi'_3$) are between 2-12, 1-11 and 3-10 subsites respectively.

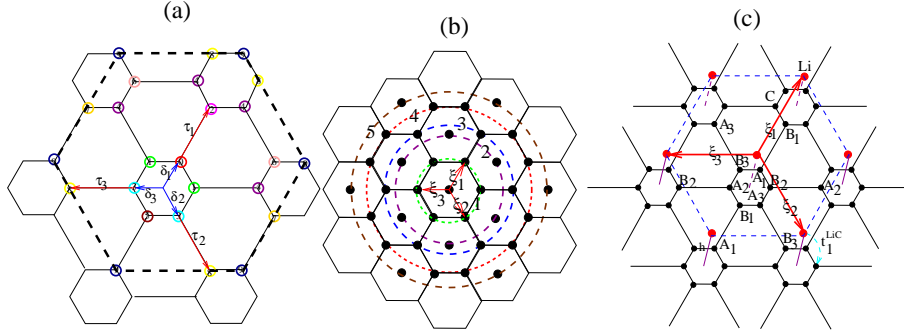


FIG. 2: Notation. (a) Shrunken single layer graphene, where numbers indicate C-C first, second, and so on, neighbors of reference carbon atom in each layer. (b) Ca sheet where nearest neighbors of a Ca atom lie on a circle with its center on Ca. (c) Graphene decorated by Ca. Distance are $a_{1c-c} = |\delta_1|$, $a_{2c-c} = |\tau_1|$.

II introduces the model Hamiltonian that we study, with Sec. III setting the stage by obtaining mostly analytic diagonalization of the non-interacting system. The treatment of pairing and presentation of superconducting phases is presented in Sec. IV, followed by a discussion and summary in Sec. V. Many of the analytic expressions are delegated to Appendices.

II. MODEL HAMILTONIAN

The system we consider, illustrated in Fig.1(a), consists of AA stacked bilayer graphene intercalated by Ca metal layer in which intercalant atoms are located on the central symmetry plane of bilayer graphene at the center of neighboring carbon hexagons. The distance between the graphene layers is calculated to be $h = 4.63\text{\AA}$ in the case of Ca intercalation. The nearest in-plane Ca-Ca distance is $\xi = 4.26\text{\AA}$. Charge transfer from Ca to the graphene layers leads to breaking symmetries of hopping amplitudes, and of C-C bond lengths similarly to those of Li decorated monolayer graphene^[9]. The attractive interaction between metal cations and C atoms after charge transfer contracts the Ca-C distance and reduces the C-C bond lengths in the Ca-centered hexagon to $a_1 = 1.419\text{\AA}$. As a result the bond length of neighboring C atoms in different hexagons is somewhat larger, at $a_2 = 1.423\text{\AA}$. Also in this “shrunk bilayer graphene”⁹ the hopping integrals between short-bond inter- and intra-layer carbons are respectively t_1^{11} and t_1^{12} , while those between stretched carbon sites will be denoted $t_1^{\prime 11}$ and $t_1^{\prime 12}$. The lattice then becomes a two dimensional hexagonal Bravais lattice with thirteen atomic sites. The sites of i -th cell will be labeled as $A_{i1}^m, A_{i2}^m, A_{i3}^m, B_{i1}^m, B_{i2}^m, B_{i3}^m$ and C_i , where m is layer index and takes $m = 1, 2$, as illustrated in Fig.2.

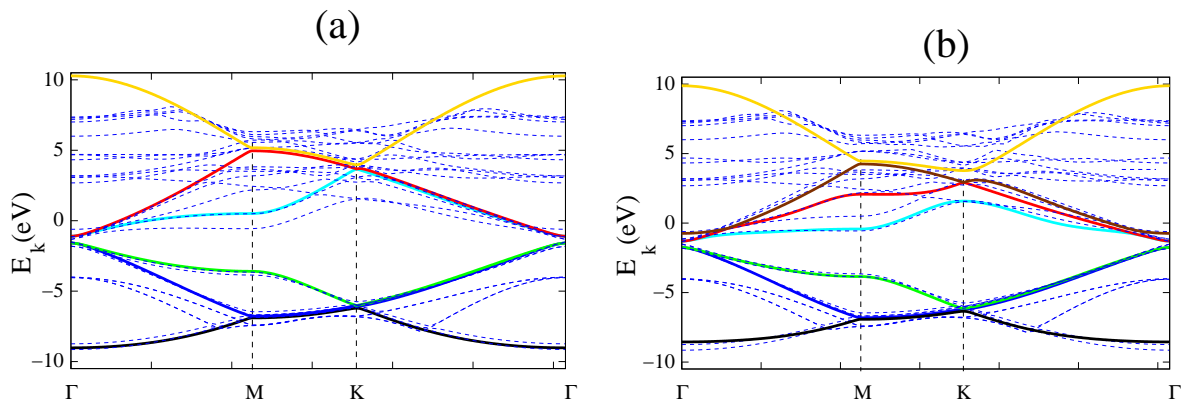


FIG. 3: Band structure of C_6CaC_6 . Left panel: bands emphasizing the six pseudo-graphene layer bands ($H^-(\vec{k})$). Right panel: emphasis on the seven pseudo-graphene layer bands ($H^+(\vec{k})$). Thin lines indicate the DFT bands, while the fitted bands are shown in color.

The Hamiltonian of this system is

$$\hat{H} = - \sum_{i\alpha} \sum_{j\beta, \sigma} t_{i\alpha, j\beta}^{\sigma, \sigma'} \hat{c}_{i\alpha\sigma}^\dagger \hat{c}_{j\beta\sigma} + \sum_{i\alpha, \sigma} (\epsilon_{i\alpha} - \mu_0) \hat{n}_{i\alpha\sigma} + \frac{1}{2} \sum_{i\alpha, \sigma} \sum_{j\beta, \sigma'} U_{i\alpha, j\beta}^{\sigma, \sigma'} \hat{n}_{i\alpha\sigma} \hat{n}_{j\beta\sigma'} = \hat{H}_N + \hat{H}_P. \quad (1)$$

where α and β run over the sublattice orbitals $A_i^m p_z$, $B_i^m p_z$ and Ca s . Here $\hat{c}_{i\alpha\sigma}^\dagger$, $\hat{c}_{i\alpha\sigma}$ are creation and annihilation operators of an electron with spin σ on subsite α of i th lattice site, and $\hat{n}_{i\sigma} = \hat{c}_{i\sigma}^\dagger \hat{c}_{i\sigma}$ is the electron number operator. The chemical potential is μ_0 and $t_{i\alpha, j\beta}$ is the hopping integral from α subsite of i th site to the β subsite of j th site. Here U is an effective negative interaction between electrons in the extended (negative U) Hubbard model that allows the possibility of superconductivity.

Section II describes the model and resulting Hamiltonian in detail. In section III we first calculate the non-interacting normal system band structure, then fit the parameters to the density functional theory (DFT) band structure. The electron interaction energy of the system is taken into account in Sec. IV in the calculation of the quasiparticle energy spectrum and superconductor pairing symmetries. Section V provides a discussion, comparison with related work, and summarizing comments.

III. THE NON-INTERACTING SYSTEM

A. Analytic Tight Binding Model for Intercalated Bilayer Graphene

In this section a thirteen band tight binding model, consisting of twelve p_z C orbitals and the Ca s orbital, for Ca-intercalated bilayer graphene is constructed, to be applied to study superconducting states of this system within BCS theory. From the beginning, the Hamiltonian is generalized to incorporate several broken symmetries, including the on-site energies, hopping integrals, and bonds lengths (geometry). Due to this generalization, it can be used to obtain analytic dispersion energies of not only C_6CaC_6 , but also related graphene-like structures such as $B_3N_3CaB_3N_3$.

The Hamiltonian of such a non-interacting system is

$$\hat{H}_N = - \sum_{i\alpha} \sum_{j\beta, \sigma} t_{i\alpha, j\beta}^{\sigma, \sigma'} \hat{c}_{i\alpha\sigma}^\dagger \hat{c}_{j\beta\sigma} + \sum_{i\alpha, \sigma} (\epsilon_{i\alpha} - \mu_0) \hat{n}_{i\alpha\sigma}. \quad (2)$$

where α and β run over sublattice orbitals A_i^m , B_i^m and the intercalated atom (e.g. Ca) orbital. The Schrödinger equation for this system in terms of Bloch coefficients in \vec{k} space becomes

$$\sum_{\beta=0}^{12} \epsilon_{\alpha\beta}(\vec{k}) \mathcal{C}_\beta + (\epsilon_\alpha - \mu_0) \mathcal{C}_\alpha = E(\vec{k}) \mathcal{C}_\alpha \quad \text{where} \quad \epsilon_{\alpha\beta}(\vec{k}) = -\frac{1}{N} \sum_{ij} e^{i\vec{k} \cdot (\vec{r}_{i\alpha} - \vec{r}_{j\beta})} t_{i\alpha, j\beta}^{\sigma\sigma}. \quad (3)$$

Here the $\beta=0, 1, 2, \dots, 12$ subscripts refer respectively to intercalant Ca, A_1^1 , A_2^1 , A_3^1 , B_1^1 , B_2^1 , B_3^1 , A_1^2 , A_2^2 , A_3^2 , B_1^2 , B_2^2 and B_3^2 . Here $\epsilon_{A_i} = \epsilon_A$ and $\epsilon_{B_i} = \epsilon_B$.

Mirror symmetry of this system result in the relations

$$\mathcal{C}_\alpha(\vec{k}) = \pm \mathcal{C}_{\alpha+6}(\vec{k}), \quad \alpha = 1, 2, \dots, 6 \quad (4)$$

which reflects the mirror symmetry through the Ca plane that separates even and odd states (positive and negative eigenvalues of the mirror operation). By inserting Eq. 4 into Eq. 3, with more detail given in Appendix A, one obtains two independent Schrödinger equations corresponding to eigenvectors $\Psi_i^-(\vec{k})^T = (0, \mathbf{C}_i(\vec{k}), -\mathbf{C}_i(\vec{k}))$, $\Psi_j^+(\vec{k})^T = (\mathcal{C}_0(\vec{k}), \mathbf{C}_j(\vec{k}), +\mathbf{C}_j(\vec{k}))$ respectively. For the odd eigensystem, the Schrödinger Eq.28 reduces to following 6×6 matrix eigenvalue problem

$$H^-(\vec{k})\mathbf{C}_n(\vec{k}) = (H_{11} - H_{12})\mathbf{C}_n(\vec{k}) = E_n^-\mathbf{C}_n(\vec{k}), \quad n = 1, 2, \dots, 6. \quad (5)$$

The Schrödinger Eq. 5 can be solved analytically, with the six eigenvalues presented in Appendix I, Eq. 44. These expressions are unaffected by the intercalant layer due to the separation of even and odd mirror symmetries, but the presence of Ca will renormalize parameters. For the even mirror sector, the Schrödinger equation Eq.28 reduces to the following 7×7 matrix eigenvalue problem

$$H_c^+(\vec{k}) \begin{pmatrix} \mathcal{C}_0(\vec{k}) \\ \sqrt{2}\mathbf{C}_n(\vec{k}) \end{pmatrix} = \begin{bmatrix} h_0(\vec{k}) & \sqrt{2}h_{01}(\vec{k}) \\ \sqrt{2}h_{10}(\vec{k}) & H^+(\vec{k}) \end{bmatrix} \begin{pmatrix} \mathcal{C}_0(\vec{k}) \\ \sqrt{2}\mathbf{C}_n(\vec{k}) \end{pmatrix} = E_n^+ \begin{pmatrix} \mathcal{C}_0(\vec{k}) \\ \sqrt{2}\mathbf{C}_n(\vec{k}) \end{pmatrix}, \quad (6)$$

where $n = 7, \dots, 13$. The other seven bands of the Schrödinger equation Eq. 28 can be obtained from solving the new Schrödinger Eq. 6. The k-dependent part of corresponding matrix components of H_{11} and H_{12} are identical in form, differing only in hopping parameters, hence $H^\pm(\vec{k})$ can be considered as a shrunken graphene monolayer Hamiltonian with renormalized hopping parameters. It follows that intercalated bilayer graphene can be interpreted as two independent pseudo-graphene monolayers where one of them is dressed by a modified hopping Ca layer. The thirteen bands of bilayer graphene divide into two groups, six bands group (odd symmetries) corresponding to H^- Hamiltonian and seven bands group (even symmetries) which are eigenvalues of H_c^+ matrix.

Mathematically many of the results obtained in Ref. [9] can be generalized to these graphene like structures but with renormalized hopping parameters. For general \vec{k} , except at Γ , it is challenging to obtain an exact analytical solution of the Schrödinger equations of Eq. 6. At the graphene Dirac points which have become folded back to the this supercell Γ point, symmetry breaking of nearest neighbor inter- and intralayer hopping parameters results in two unequal small gaps with different centers, corresponding to six and seven band pseudo-graphene Hamiltonians, given by

$$E_g^\pm = 2|(t_{11} - t'_{11}) \pm (t_{12} - t'_{12})|. \quad (7)$$

Analytic solutions of Eq. 6 result in the event that intercalant layer hopping parameters to graphene sheets are negligible, as in the case of Li-decorated graphene where Li atoms fully ionize and the Li-associate band lies above the Fermi energy, so Li-C hopping effects are negligible. In this particular case the odd (-) and the even (+) nontrivial eigenvalues of H^\pm matrix, are given by

$$E_{sh,m,l}^\pm(t_i, \vec{\xi}_i, \vec{k}) = \mu_m^\pm(\vec{k}) - \mu_o + \frac{1}{2} \left[\varepsilon_A + \varepsilon_B + (-1)^l \sqrt{(\varepsilon_A - \varepsilon_B)^2 + 4w_m^\pm(t_i, \vec{\xi}_i, \vec{k})} \right], \quad m = 1, 2, 3; l = 1, 2 \quad (8)$$

Details for obtaining these results are presented in Appendix A and Ref. [9]. $\mu_m^\pm(\vec{k})$, $w_m^\pm(t_i, \vec{\xi}_i, \vec{k})$ are defined in Eqs. 45 and 48 respectively.

Now further notation is established. This transformation rearranges the noninteracting Hamiltonian Eq. 2 as the direct sum of two single layer pseudo-graphene structures with renormalized hopping integrals of the form

$$\hat{H}_N = \hat{H}_N^+ \oplus \hat{H}_N^- = \sum_{ij\sigma} \sum_{\alpha,\beta=0}^6 t_{i\alpha\sigma,j\beta\sigma}^+ \hat{c}_{i\alpha\sigma}^{+\dagger} \hat{c}_{j\beta\sigma}^+ \oplus \sum_{ij\sigma} \sum_{\alpha,\beta=1}^6 t_{i\alpha\sigma,j\beta\sigma}^- \hat{c}_{i\alpha\sigma}^{-\dagger} \hat{c}_{j\beta\sigma}^- \quad (9)$$

wherein, as illustrated in Fig.1(b), we introduced quasiparticle creation operators and hopping integrals in real space,

$$\hat{c}_{i\alpha\sigma}^{(\pm)\dagger} = \frac{1}{\sqrt{2}}(\hat{c}_{i\alpha\sigma}^\dagger \pm \hat{c}_{i,\alpha+6,\sigma}^\dagger), \quad t_{i\alpha\sigma,j\beta\sigma}^\pm = t_{i\alpha\sigma,j\beta\sigma}^{inter} \pm t_{i\alpha\sigma,j\beta+6\sigma}^{intra}, \quad \alpha, \beta = 1, \dots, 6. \quad (10)$$

The creation operator $\hat{c}_{i\alpha\sigma}^{(\pm)\dagger}$ creates an electron in a linear combination of the spin-parallel (σ) atomic states of the bilayer system, directly in the formation of superconducting phases.

The separation of thirteen bands of intercalated bilayer graphene into groups of six odd-symmetry and seven-even symmetry bands has strong advantages. The tight-binding model band structures can be fit to DFT band structure results with greater accuracy and simplicity, for example. Especially when the pairing interactions are introduced, this transformation reduces the speed of numerical calculations significantly and provides additional insight into physical properties of bilayer graphene.

B. Fit to DFT band structures

This formalism has been applied and divided into two separated effective single layer (shrunk)- pseudo-graphene models. The six odd bands and seven even bands were fit to DFT bands with results shown in Fig. 3. The reduced fitting parameters are given in Tables I and II.

We follow the model presented in Ref. [9]. As illustrated in Fig. 1(a) and Fig. 2(a),(c) on each of bilayer graphene sheets, the A_1 sublattice site of the central unit cell is chosen as the origin labeled by 0, and the B_1 site in the adjacent hexagon is considered as the second C atom neighbor. While just slightly longer than the first neighbors atoms B_2 and B_3 in the same hexagon, this neighbor is labeled by $n = 2$, and so on the further neighbors are labeled. In Fig. 2 (a), the big dashed hexagon included up to nine intra-plane neighbors but for the pristine graphene it is surrounded by five neighbors. C-C hopping from 0-subsite to intra-plane n th neighbor (t_{i0jn}^{intra}) plus (minus) hopping from 0-subsite to inter-plane n th neighbor (t_{0n}^{inter}) has been shown by $t_{0n}^{\pm CC}$. In-plane Ca-Ca hoppings t_{0m}^{Ca-Ca} are included up to $m = 4$ neighbors. Modified Ca to C hopping integrals in Eq. 6, which are defined as $\sqrt{2}$ times the hopping from central Ca to m th neighbor C atoms, are denoted by t_{0m}^{CaC} and obtained up to $m = 5$ neighbors.

The six odd bands and seven even bands specified by Eqs. 5 and 6 respectively, have reduced hopping integrals given by $t_{im\sigma,jn\sigma}^{\pm} = t_{im,jn}^{inter} \pm t_{im,jn}^{intra}$, DFT calculated bands were fitted to tight binding odd bands of Eq. 8, with results presented in Fig. 3(a) and Table I. The even bands which are solutions of Eq. 6 are obtained numerically and fitted to the DFT bands. The results are illustrated in Fig. 3(b) and Table II.

There are two flat bands with d -wave Bloch character: one in each of the odd and even sectors. The opposite signs of nearest neighbor inter- and intra-layer hopping amplitudes, t_1^{11} and t_1^{12} , leads to reduced bandwidths of the even states (+ sign) in Eq. 6. Larger interlayer hopping t_1^{12} leads to smaller bandwidth ($H^{\pm} = H_{11} \pm H_{12}$), while for the other six odd-symmetry bands, the bandwidth can increase as can be seen in Fig. 3. On the other hand, the bandwidth of the even sector flat band is reduced, again due to the calcium to carbon hopping while the odd sector is not affected by Ca-C hoppings. For this reason, the flat band belonging to the even-seven bands group plays a major role in superconductivity.

TABLE I: The C-C hopping parameters (in eV) for the six odd symmetry bands of C_6CaC_6 are denoted by $t_{0n}^{(-)CC}$ where the index n indicates n -th neighbour.

n	0	1	2	3	4	5	6	7	8	9
$t_{0n}^{(-)CC}$	$\epsilon_c^- = -1.00$	$t_1^- = 3.04$	$t_1'^- = 0.92t_1^-$	$t_2^- = -0.23$	$t_2'^- = 0.92t_2^-$	$t_3^- = -0.29$	$t_3'^- \approx t_3^-$	$t_4^- = -0.02$	$t_4'^- \approx t_4^-$	$t_5^- = -0.05$

TABLE II: The C-C hopping parameters (in eV) for the seven even-symmetry bands of C_6CaC_6 are denoted by $t_{0n}^{(+)CC}$ where the index n indicates the n -th neighbour. In the intercalant plane, Ca-Ca hopping parameters are denoted by t_{0m}^{CaCa} where m is m -th Ca neighbor of central Ca. The modified Ca-C hopping parameter is t_{0m}^{CaC} .

n	0	1	2	3	4	5	6	7	8	9
$t_{0n}^{(+)CC}$	$\epsilon_c^+ = -0.60$	$t_1^+ = 2.94$	$t_1'^+ = 0.92t_1^+$	$t_2^+ = -0.24$	$t_2'^+ = 0.92t_2^+$	$t_3^+ = 0.27$	$t_3'^+ \approx t_3^+$	$t_4^+ = -0.02$	$t_4'^+ \approx t_4^+$	$t_5^+ = -0.08$
m	0	1	2	3	4	5				
t_{0m}^{CaCa}	$\epsilon_{Ca} = 1.12$	-0.35	0.06	0.06	-0.02	0.00				
t_{0m}^{CaC}	-	0.17	-0.14	0.08	-0.07	-0.05				

IV. SUPERCONDUCTING PAIRING AND STATES

A. Bogoliubov-de Gennes Transformation

We treat the thirteen band Hubbard model in mean field approximation to investigate superconductivity in intercalated bilayer graphene. Singlet pairing is considered and, as illustrated in Fig. 1, pairing interactions are pictured in real space as interactions between nearest neighbors on inter- and intra-layer carbon atoms. This superconducting Hamiltonian can be transformed, as for the non-interacting case, to the direct sum of two independent superconducting Hamiltonian corresponding to odd and even symmetries pseudo-graphene structures

$$\hat{H}_{su} = \sum_{\vec{k}} \Lambda^\dagger(\vec{k}) \begin{pmatrix} H_{su}^+(\vec{k}) & 0 \\ 0 & H_{su}^-(\vec{k}) \end{pmatrix} \Lambda(\vec{k}) \quad (11)$$

where $\Lambda^\dagger(\vec{k}) = \left([\hat{c}_{0\uparrow}^\dagger(\vec{k}) \hat{c}_{1\uparrow}^\dagger(\vec{k}) \dots \hat{c}_{6\uparrow}^\dagger(\vec{k}) \hat{c}_{0\downarrow}(-\vec{k}) \hat{c}_{1\downarrow}(-\vec{k}) \dots \hat{c}_{6\downarrow}(-\vec{k})] \quad [\hat{c}_{1\uparrow}^\dagger(\vec{k}) \hat{c}_{2\uparrow}^\dagger(\vec{k}) \dots \hat{c}_{6\uparrow}^\dagger(\vec{k}) \hat{c}_{1\downarrow}(-\vec{k}) \hat{c}_{2\downarrow}(-\vec{k}) \dots \hat{c}_{6\downarrow}(-\vec{k})] \right)$, in which $\hat{c}_{m\sigma}^{(\pm)\dagger}(\vec{k}) = \frac{1}{\sqrt{2}}(\hat{c}_{m\sigma}^\dagger(\vec{k}) \pm \hat{c}_{m+6,\sigma}^\dagger(\vec{k}))$ and H_{su}^+ and H_{su}^- are Hamiltonians of even and odd symmetry pseudo-graphene structures respectively; for more information see Appendix C. Decoupling of these Hamiltonians means there is no effective pairing between an electron in the even sector with one in the odd sector. Using the fact that the gap is small on the electronic scale, applying perturbation up to second order gives quasiparticle energies from Eq.11 (see Ref. [9]) as

$$E_{m,s}^{Q+}(\vec{k}) = s \left(E_m^+(\vec{k}) + \sum_{n=1}^7 \frac{|\Delta_{mn}^+(\vec{k})|^2}{E_m^+(\vec{k}) + E_n^+(\vec{k})} \right), \quad \Delta_{mn}^+(\vec{k}) = \sum_{\alpha=1}^9 \Omega_{mn}^{+\alpha}(\vec{k}) \Delta_+^\alpha \quad s = \pm 1, \quad m = 1, 2, \dots, 7 \quad (12)$$

$$E_{m,s}^{Q-}(\vec{k}) = s \left(E_m^-(\vec{k}) + \sum_{n=8}^{13} \frac{|\Delta_{mn}^-(\vec{k})|^2}{E_m^-(\vec{k}) + E_n^-(\vec{k})} \right), \quad \Delta_{mn}^-(\vec{k}) = \sum_{\alpha=1}^9 \Omega_{mn}^{-\alpha}(\vec{k}) \Delta_-^\alpha \quad s = \pm 1, \quad m = 8, 9, \dots, 13 \quad (13)$$

Here $(\Delta_\pm^1 \quad \Delta_\pm^2 \quad \Delta_\pm^3) = [(g_1 \Sigma_1 \pm g'_1 \Sigma'_1) \quad (g_1 \Sigma_2 \pm g'_1 \Sigma'_2) \quad (g_1 \Sigma_3 \pm g'_1 \Sigma'_3)]$, $(\Delta_\pm^4 \quad \Delta_\pm^5 \quad \Delta_\pm^6) = [(g_0 \Delta_1 \pm g'_0 \Delta'_1) \quad (g_0 \Delta_2 \pm g'_0 \Delta'_2) \quad (g_0 \Delta_3 \pm g'_0 \Delta'_3)]$ and $(\Delta_\pm^7 \quad \Delta_\pm^8 \quad \Delta_\pm^9) = [(g_0 \Pi_1 \pm g'_0 \Pi'_1) \quad (g_0 \Pi_2 \pm g'_0 \Pi'_2) \quad (g_0 \Pi_3 \pm g'_0 \Pi'_3)]$, where $\langle ij \rangle$ subscript has been dropped for brevity. Also

$$\begin{aligned} \Omega_{mn}^{1\pm}(\vec{k}) &= \mathcal{C}_1^*(E_m^\pm) \mathcal{C}_4(E_n^\pm) e^{i\vec{k} \cdot \vec{\tau}_1} + \mathcal{C}_4^*(E_m^\pm) \mathcal{C}_1(E_n^\pm) e^{-i\vec{k} \cdot \vec{\tau}_1} \\ \Omega_{mn}^{2\pm}(\vec{k}) &= \mathcal{C}_3^*(E_m^\pm) \mathcal{C}_6(E_n^\pm) e^{i\vec{k} \cdot \vec{\tau}_2} + \mathcal{C}_6^*(E_m^\pm) \mathcal{C}_3(E_n^\pm) e^{-i\vec{k} \cdot \vec{\tau}_2} \\ \Omega_{mn}^{3\pm}(\vec{k}) &= \mathcal{C}_2^*(E_m^\pm) \mathcal{C}_5(E_n^\pm) e^{i\vec{k} \cdot \vec{\tau}_3} + \mathcal{C}_5^*(E_m^\pm) \mathcal{C}_2(E_n^\pm) e^{-i\vec{k} \cdot \vec{\tau}_3} \\ \Omega_{mn}^{4\pm}(\vec{k}) &= \mathcal{C}_2^*(E_m^\pm) \mathcal{C}_6(E_n^\pm) e^{i\vec{k} \cdot \vec{\delta}_1} + \mathcal{C}_6^*(E_m^\pm) \mathcal{C}_2(E_n^\pm) e^{-i\vec{k} \cdot \vec{\delta}_1} \\ \Omega_{mn}^{5\pm}(\vec{k}) &= \mathcal{C}_1^*(E_m^\pm) \mathcal{C}_5(E_n^\pm) e^{i\vec{k} \cdot \vec{\delta}_2} + \mathcal{C}_5^*(E_m^\pm) \mathcal{C}_1(E_n^\pm) e^{-i\vec{k} \cdot \vec{\delta}_2} \\ \Omega_{mn}^{6\pm}(\vec{k}) &= \mathcal{C}_3^*(E_m^\pm) \mathcal{C}_4(E_n^\pm) e^{i\vec{k} \cdot \vec{\delta}_3} + \mathcal{C}_4^*(E_m^\pm) \mathcal{C}_3(E_n^\pm) e^{-i\vec{k} \cdot \vec{\delta}_3} \\ \Omega_{mn}^{7\pm}(\vec{k}) &= \mathcal{C}_3^*(E_m^\pm) \mathcal{C}_5(E_n^\pm) e^{i\vec{k} \cdot \vec{\delta}_1} + \mathcal{C}_5^*(E_m^\pm) \mathcal{C}_3(E_n^\pm) e^{-i\vec{k} \cdot \vec{\delta}_1} \\ \Omega_{mn}^{8\pm}(\vec{k}) &= \mathcal{C}_2^*(E_m^\pm) \mathcal{C}_4(E_n^\pm) e^{i\vec{k} \cdot \vec{\delta}_2} + \mathcal{C}_4^*(E_m^\pm) \mathcal{C}_2(E_n^\pm) e^{-i\vec{k} \cdot \vec{\delta}_2} \\ \Omega_{mn}^{9\pm}(\vec{k}) &= \mathcal{C}_1^*(E_m^\pm) \mathcal{C}_6(E_n^\pm) e^{i\vec{k} \cdot \vec{\delta}_3} + \mathcal{C}_6^*(E_m^\pm) \mathcal{C}_1(E_n^\pm) e^{-i\vec{k} \cdot \vec{\delta}_3}. \end{aligned} \quad (14)$$

Here $\mathcal{C}_m(E_n^-)$ is the m th component of n th column eigenvector of H^- and $\mathcal{C}_m(E_n^+)$ is $(m+1)$ th component of n th eigenvector of $H_c^+(\vec{k})$. Band order parameters $\Delta_{mn}^+(\vec{k})$ are defined such that first electron is in the m th band and second electron is in the n th band of $H_c^+(\vec{k})$, also $\Delta_{mn}^-(\vec{k})$ is defined such that first electron is in the m th band and second electron is in the n th band of $H^-(\vec{k})$. Note that an electron in the m th band of $H_c^+(\vec{k})$ and an electron in n th band of $H^-(\vec{k})$ cannot be paired; *i.e.* for this case $\Delta_{mn}^\pm(\vec{k}) = 0$.

The Bogoliubov-de Gennes transformation used in Eq. 11 shows that pairing amplitudes should be $\Delta_\pm^\alpha = \langle \hat{c}_{\alpha,i}^\pm \hat{c}_{\alpha,j}^\pm \rangle$ which implies that all inter- and intra-layer pairing amplitudes in real space are equal, $g_0 = g'_0$ and $g_1 = g'_1$. This

restriction makes the matrix gap equations hermitian and implies that band order parameters, $\Delta_{mn}^{\pm}(\vec{k})$ can be interpreted physically as pairing of electrons in different bands with pairing interaction g_0^{\pm} . In this limit $\Delta_{mn}^{\pm}(\vec{k})$ is equal to the product of band Green function and g_0 ,

$$\Delta_{mn}^{\pm}(\vec{k}) = g_0^{\pm} \langle \hat{d}_m^{\pm\uparrow}(\vec{k}) \hat{d}_n^{\pm\downarrow}(\vec{k}) \rangle \quad (15)$$

where $\hat{d}_i^{\pm\sigma}(\vec{k}) = \sum_{m=1}^7 \mathcal{C}_m^{\pm*}(E_i(\vec{k})) \hat{c}_m^{\sigma}(\vec{k})$ annihilates an electron with spin σ in the i th even or odd bands with energy $E_i^{\pm}(\vec{k})$.

B. Two Gap Superconducting Pairings and States

The linearized gap equation can be decoupled by minimizing free energy with respect to nearest neighbor pairing, or equivalently with respect to Δ_{\pm}^{α} , for more detail see Appendix C. Minimization of free energy with respect to Δ_{\pm}^{α} gives

$$\begin{bmatrix} A^{\pm} & B^{\pm} & B^{\pm} \\ B^{\pm} & C^{\pm} & D^{\pm} \\ B^{\pm} & D^{\pm} & C^{\pm} \end{bmatrix} \begin{pmatrix} \Sigma_i \pm \Sigma'_i \\ \Pi_i \pm \Pi'_i \\ \Delta_i \pm \Delta'_i \end{pmatrix} = -\frac{1}{g_0^{\pm}} \begin{pmatrix} \Sigma_i \pm \Sigma'_i \\ \Pi_i \pm \Pi'_i \\ \Delta_i \pm \Delta'_i \end{pmatrix} \quad (16)$$

in which A , B , C and D matrices have been introduced as

$$A^{\pm} = \begin{bmatrix} \Gamma_{11}^{\pm} & \Gamma_{12}^{\pm} & \Gamma_{12}^{\pm} \\ \Gamma_{12}^{\pm} & \Gamma_{11}^{\pm} & \Gamma_{12}^{\pm} \\ \Gamma_{12}^{\pm} & \Gamma_{12}^{\pm} & \Gamma_{11}^{\pm} \end{bmatrix}, \quad C^{\pm} = \begin{bmatrix} \Gamma_{44}^{\pm} & \Gamma_{45}^{\pm} & \Gamma_{45}^{\pm} \\ \Gamma_{45}^{\pm} & \Gamma_{44}^{\pm} & \Gamma_{45}^{\pm} \\ \Gamma_{45}^{\pm} & \Gamma_{45}^{\pm} & \Gamma_{44}^{\pm} \end{bmatrix}, \quad B^{\pm} = \begin{bmatrix} \Gamma_{14}^{\pm} & \Gamma_{15}^{\pm} & \Gamma_{15}^{\pm} \\ \Gamma_{15}^{\pm} & \Gamma_{14}^{\pm} & \Gamma_{15}^{\pm} \\ \Gamma_{15}^{\pm} & \Gamma_{15}^{\pm} & \Gamma_{14}^{\pm} \end{bmatrix}, \quad D^{\pm} = \begin{bmatrix} \Gamma_{47}^{\pm} & \Gamma_{48}^{\pm} & \Gamma_{48}^{\pm} \\ \Gamma_{48}^{\pm} & \Gamma_{47}^{\pm} & \Gamma_{48}^{\pm} \\ \Gamma_{48}^{\pm} & \Gamma_{48}^{\pm} & \Gamma_{47}^{\pm} \end{bmatrix}. \quad (17)$$

wherein, Γ matrix elements are given by

$$\Gamma_{\beta\alpha}^{\pm} = \frac{1}{N} \sum_{\vec{k}} \sum_i \sum_j \frac{\tanh(\frac{E_i^{\pm}}{2k_B T})}{E_j^{\pm}(\vec{k}) + E_i^{\pm}(\vec{k})} \left(\Omega_{ij}^{\pm\alpha}(\vec{k}) \Omega_{ji}^{\pm\beta}(\vec{k}) + \Omega_{ji}^{\pm\alpha}(\vec{k}) \Omega_{ij}^{\pm\beta}(\vec{k}) \right). \quad (18)$$

Equation 16 can be interpreted as two independent gap equations for odd (minus sign) and even (plus sign) pseudo-graphene systems. The impact is that superconductivity can be established independently in two distinct sectors this system. In the next section we numerically inspect which of these pseudo-graphene sectors, odd or even, play major rules of superconductivity.

Gholami *et al.*⁹ solved such gap equations for Li-decorated single layer graphene. The gap equations in Eq. 63 are the same form so they can be solved similarly. The A , B , C , and D matrices have identical structures, hence they share eigenvectors: $V_s^T = (1 \ 1 \ 1)$, $V_{d_{xy}}^T = (1 \ -1 \ 0)$, and $V_{d_{x^2-y^2}}^T = (1 \ 1 \ -2)$, where the latter two are degenerate. Their eigenvalues, in obvious notation, are

$$\begin{aligned} a_s^{\pm} &= \Gamma_{11}^{\pm} + 2\Gamma_{12}^{\pm}, & b_s^{\pm} &= \Gamma_{14}^{\pm} + 2\Gamma_{15}^{\pm}, & c_s^{\pm} &= \Gamma_{44}^{\pm} + 2\Gamma_{45}^{\pm}, & d_s^{\pm} &= \Gamma_{47}^{\pm} + 2\Gamma_{48}^{\pm} \\ a_d^{\pm} &= \Gamma_{11}^{\pm} - \Gamma_{12}^{\pm}, & b_d^{\pm} &= \Gamma_{14}^{\pm} - \Gamma_{15}^{\pm}, & c_d^{\pm} &= \Gamma_{44}^{\pm} - \Gamma_{45}^{\pm}, & d_d^{\pm} &= \Gamma_{47}^{\pm} - \Gamma_{48}^{\pm}. \end{aligned} \quad (19)$$

Similar to decorated single layer graphene⁹, for each of the gap equations given by Eq. 63 there are nine independent solutions. The first three superconducting states with island (localized) character can be expressed in compact form as

$$[\Psi_{\Delta_{sy}^{\pm}}^0]^T = [0, \quad V_{sy}, \quad -V_{sy}], \quad J_{sy}^{0\pm} = c_{sy}^{\pm} - d_{sy}^{\pm} \quad (20)$$

where V_{sy} refers to one of the V_s , $V_{d_{xy}}$ or $V_{d_{x^2-y^2}}$ -wave symmetries. Pairing in these phases cannot propagate. The other six superconducting states of Eq. 63 have the explicit form

$$[\Psi_{\Delta_{sy}^{\pm}}^l]^T = [\alpha_{sy}^{l,\pm} V_{sy}, \quad V_{sy}, \quad V_{sy}] \quad (21)$$

where

$$\alpha_{sy}^{l,\pm} = \frac{J_{sy}^{l,\pm} - c_{sy}^{\pm} - d_{sy}^{\pm}}{b_{sy}^{\pm}}, \quad J_{sy}^{l,\pm} = \frac{1}{2} \left(a_{sy}^{\pm} + c_{sy}^{\pm} + d_{sy}^{\pm} + (-1)^l \sqrt{8(b_{sy}^{\pm})^2 + [c_{sy}^{\pm} + d_{sy}^{\pm} - a_{sy}^{\pm}]^2} \right), \quad l = 1, 2. \quad (22)$$

Here $c_{sy} = c_s^\pm, c_d^\pm$, $b_{sy} = b_s^\pm, b_d^\pm$, $d_{sy} = d_s, d_d^\pm$ and $J_{sy}^{l,\pm} = -\frac{1}{g_0^\pm}$ for each symmetry, and + superscript refer to the even sector and - superscripts to the odd sector. In each of above categories, $d_{x^2-y^2}$ and d_{xy} phases are degenerate. Similar to decorated single layer graphene, only three of solutions for which $l = 2$ are physically reachable in the framework of mean field theory. In the limit of pristine bilayer graphene, these three states convert to usual s-wave and d-wave symmetries. In the next section, for odd and even sectors we illustrate from numerical solutions which of these three phases are dominant.

C. Flat band(s) Superconductivity: Strong interlayer coupling

As shown in Fig. 3, two conduction bands corresponding to odd and even sector are weakly dispersive near the Fermi energy along $\Gamma \rightarrow M$, which seems to play a major role in the formation of superconducting Cooper's pairs. Recently unconventional superconductivity has been reported in twisted bilayer graphene in which the two layers are twisted with respect to each other at certain "magic" angle. At this angle, the band we talk about suddenly becomes flat. To make a rough estimate and provide mathematical insight into the physics, one can diagonalize normal state Hamiltonian of pristine bilayer graphene in the mini-Brillouin zone of C_6CaC_6 . The Brillouin zone (BZ) of C_6 is one third of that of graphene, with the Dirac points folded back to the Γ point. In this mini-BZ, the two π bands of odd and even pristine pseudo-graphene folds to six branches and their different symmetries are also separated as illustrated in Fig. 2 of Ref. [9]. These branches and their corresponding Bloch wave functions are given by Eqs. 39, 40, 41, and 42.

In the case of pristine bilayer graphene, odd (-) and even (+) so called flat bands are the minimum of $(E_{\alpha,2}^\pm(\vec{k}), E_{\beta,2}^\pm(\vec{k}))$ along different high symmetry paths that are given by Eqs. 40 and 41, where their Bloch wave function, viz. Eq. 42, are similar to those of Ref.⁹. They have linear combination of $d_{x^2-y^2}$ and d_{xy} character and are responsible for superconducting pairing $d_{x^2-y^2}$ and d_{xy} .

One can ask: what is so special about these flat bands? To address this question, we return to the matrix gap equation of Eq. 18. The right hand side contains the product of a form factor given by $\Omega_{ni}^\alpha(\vec{k})\Omega_{ni}^{*\beta}(\vec{k}) + \Omega_{ni}^\beta(\vec{k})\Omega_{ni}^{*\alpha}(\vec{k})$ and the thermal occupation factor over the energy denominator i.e. $\frac{\tanh(\frac{E_n}{k_B T})}{E_n(\vec{k}) + E_i(\vec{k})}$. The form factor is a function of the Bloch wave coefficients of normal state Hamiltonian. Using Eqs. 42, 43 one can investigate that in the limited case of pristine bilayer graphene at the nearest neighbor approximation, these Bloch wave coefficients are the same for both sectors and this is almost for the next neighbor approximation. As such, it is independent of chemical potential μ . Thus the form factor is the same for the both odd and even sector of band structures. Since $\frac{\tanh(x)}{x} \rightarrow 1$ as $x \rightarrow 0$, when one of the conduction odd or even flat bands and so their corresponding valance bands becomes completely flat at the Fermi level then $\frac{\tanh(\frac{\beta E_i}{2})}{E_i(\vec{k}) + E_j(\vec{k})} \rightarrow \frac{\beta}{4}$, where $E_i(\vec{k})$ or $E_j(\vec{k})$ are one of these flat bands. In this case the dominant contribution comes from these mutual conduction and valance flat bands, and one can show that all gap equation block matrix elements in Eq. 17 are equal to A^\pm . In this event, depending on whether the flat bands belong to the odd or even sector, one can use Eqs. 14, 18, and 42 to show that

$$\Gamma_{11}^\pm \rightarrow \frac{\beta_c}{9}, \quad \Gamma_{12}^\pm \rightarrow -\frac{\beta_c}{36}, \quad (\beta_c = \frac{1}{k_B T_c}). \quad (23)$$

Cooper pair interaction potentials g_0 of d-wave symmetry, *i.e.* g_0^d and s-wave symmetry g_0^s , are given by

$$g_0^d = \frac{1}{3(\Gamma_{11}^\pm - \Gamma_{12}^\pm)} = \frac{12}{5} k_B T_c$$

$$g_0^s = \frac{1}{3(\Gamma_{11}^\pm + 2\Gamma_{12}^\pm)} = 6 k_B T_c \quad (24)$$

In this case $\Gamma_{12}^\pm < 0$ and g_0^d is less than g_0^s , so d-wave symmetry is dominant, with an extraordinary decrease in pairing potential interaction proportional to the critical temperature. This "ultra" decrease of pairing interaction can explain the importance of the flat bands in the formation of Cooper pairs in twisted bilayer graphene.

Another interesting point that can be deduced from mathematical calculations is that in the limit of strong interlayer hopping when inter-layer hoppings tends to minus (plus) of intra-layer hoppings, as one can see from Appendix D, all of the six bands of even (odd) sector become flat while the other sector bandwidths increases. Then one can show that the gap matrix elements are

$$\Gamma_{i,j} \rightarrow \beta_c \delta_{ij}; \quad g_0 = k_B T_c \quad (25)$$

and so all possible superconducting symmetries are degenerate with pairing potential $g_0 = k_B T_c$. This observation suggests there may be some aspect of unconventional superconductivity of twisted bilayer graphene related to inter-versus intralayer hopping effects.

V. NUMERICAL RESULTS

A. General features

To know in the variety of doping regimes which of the pairing symmetries (distorted s -wave or d -wave) are dominant, and also to inspect in the which sectors of the band structure Cooper pairs with the lowest pairing potential can be constructed, superconducting gap equations of odd and even sectors *i.e.* Eq. 16 are solved numerically. The result is shown in Fig. 4.

Similar to Li intercalated single layer graphene (Ref. [9]), at moderate doping, d -wave superconductivity always dominates in both sectors of the C_6CaC_6 band system. Distorted s -wave symmetry only survives at high doping levels. For odd and even sector flat bands, the density of states peaks at the M critical point. This point, for the odd flat band, is located about 0.5 eV above the Fermi level, and about 0.44 eV below the Fermi level for the case of the even flat band. Exploration of each of these flat bands can be engineered by applying a gate voltage on the bilayer via a change in the chemical potential μ . As illustrated in Fig. 4, around $\mu = 0$ at $T_c = 1K$ *i.e.* C_6CaC_6 is not affected by gate voltage. Dominant d -wave symmetry pairing phases are degenerate, so pairing can arise in both odd and even flat bands. This occurs when the averaged density of states of both bands are the same near the Fermi level. When the odd flat band is dominant near Fermi level due to electron doping, d -wave pairing dominates in this band, with the minimum of the pairing interaction energy ($g_0^- = 0.35$) corresponding to the M point near $\mu = 0.5eV$.

B. Hole doping

Hole doping by gating, by Ca \rightarrow Na substitution, or by Ca deficiency, leads to the situation where the even flat band dominates. Dominant d -wave symmetry occurs in this band with the lowest pairing energy ($g_0^+ = 0.12$), again at the critical M point at $\mu = -0.44eV$. From Fig. 4 it can be seen that when the even flat band is dominant (hole doping), the pairing potential g_0 of d -wave symmetry emerging from this band is less than the case that dominant d -wave symmetry occurs in the odd flat band (by electron doping). For example, with a factor of one-third at their critical M point *i.e.* $g_0^+ = \frac{1}{3}g_0^-$, that means that when the even flat band reaches near the Fermi level, reduction of bandwidth due to both interlayer C-C interaction (H_{12}) and C-Ca layer interactions lead to a sharp increase in the density of states. While both C-C and Ca-C interlayer interaction decrease the pairing potential g_0 , one can numerically inspect that reduction of the bandwidth due to graphene interlayer interaction, more affected the energy of pairing in the even flat band than Ca-C layers interaction.

In the case of Ca intercalated bilayer graphene, for a given T_c the pairing interaction potential g_0 (proportional to superconducting gap energy, $|\Delta|^2$) for dominant d -wave phases of the odd and even superconducting gaps are illustrated in Fig. 5. It is evident that for a given critical temperature T_c , superconductivity can be single gap or two gap and dominant superconducting pairings can occur between electrons in the odd H^- , or even H_c^+ , sector.

VI. DISCUSSION AND SUMMARY

Superconductivity in bilayer graphene intercalated by calcium has been reported experimentally around $T_c = 4K$.^{4,5} Applying anisotropic Migdal-Eliashberg theory based on *ab initio* calculations of electron-phonon coupling Margine *et al.* calculated⁸ that this superconductivity is a phonon mediated two-gap superconductor with predicted T_c around 7K. Recently unconventional superconductivity up to $T_c = 1.7K$ has been reported in gated twisted bilayer graphene where the layers are rotated relative to each other by a magic angle of 1.1° . Superconductivity in this low doping regime of band filling cannot be addressed within the framework of conventional electron-phonon coupling based on Migdal's adiabatic approximation. This discovery has opened speculation that this superconducting behavior may shed light on other systems in which superconductivity arises from an insulating phase.³ This development also highlights studies such as ours, which does not rely on the mechanism, but instead on more general pairing concepts and the specific electronic structure.

While experimental studies show that superconductivity occurs in the intercalated bilayer graphene in which graphene layers are AA stacked, most theoretical microscopic models of pristine honeycomb bilayer superconductivity concentrate on the more stable AB stacking of bilayer graphene.^{10,11} To our knowledge, there are no analogous

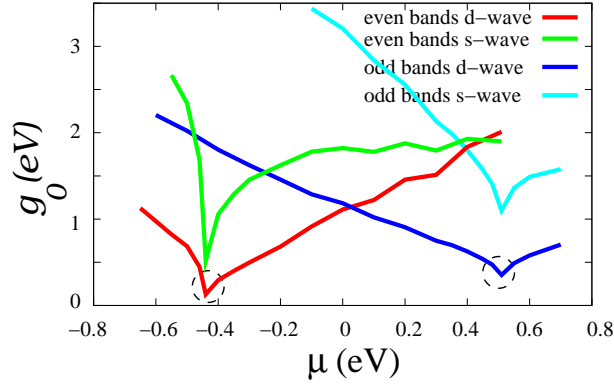


FIG. 4: Pairing interaction potential g_0 versus chemical potential μ . Both odd (six band) and even (seven band) symmetry solutions are shown for $T_c = 1K$. Their corresponding d -wave phases are degenerate around $\mu = 0$ and pairing separately contributes to a phase with two differing gaps. For both odd and even flat bands, d -wave symmetries are dominant at moderate doping, while at high doping a phase transition from d -wave to distorted s -wave occurs. This transition can be seen for the even flat band near $\mu = 0.5eV$. Hole doping causes the d -wave symmetry pairing to prevail between electrons in the even flat band case, with a minimum of pairing potential interaction $g_0^+ = 0.12eV$ where there occurs a critical M point at -0.44 eV shown by a dashed circle. Vice versa, electron doping leads to d -wave symmetry pairing between electrons in the odd flat band, with a minimum of pairing potential interaction at $g_0^+ = 0.12eV$ that occurs at the critical M point at -0.44 eV shown by a dashed circle.

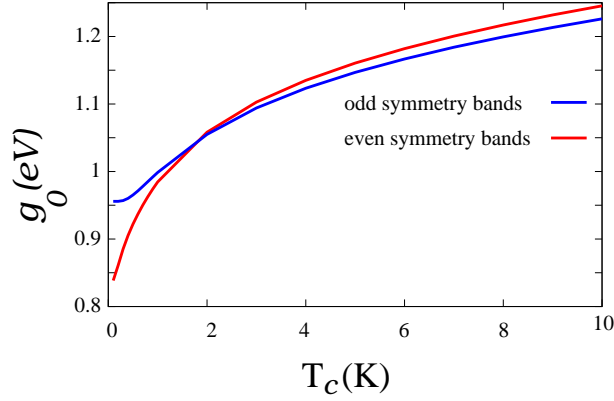


FIG. 5: Critical temperature T_c versus pairing potential g_0 . Shown are the dominant d -wave solutions of the odd (six band) and even (seven band) symmetry superconducting gap equations. At $T_c = 2K$ the phases are degenerate, and pairing separately contributes to a phase with two gaps.

studies that focus on AA stacked bilayer graphene. In Ref. [10], in the limit of strong interlayer hopping, the four-band model of AB stacked bilayer graphene may be converted to an effective artificially truncated two band monolayer honeycomb lattice Hamiltonian with nearest neighbor hopping $2\tilde{t}$, second neighbor hopping does not appear, but with third neighbor hopping $\tilde{t} = \frac{t^2}{t_+}$. In that effective model, their conclusions were that the $d + id$ superconducting instability is the leading superconducting instability of the honeycomb bilayer with strong interlayer hopping at finite doping.

In the general case and accounting for symmetries of Bloch wave coefficients, both AA and AB stacked bilayer graphene can be mapped exactly onto separate renormalized hopping, pseudo-graphene structures. In our work we have used a realistic tight binding model to investigate the superconducting phases of intercalated bilayer graphene. The 13×13 Hamiltonian of C_6CaC_6 converts, by mirror symmetry, to two effective single layer pseudo-graphene sectors: an even symmetry sector with involvement of the intercalant, and the six band odd sector for which the intercalant provides only renormalized hopping amplitudes. In both cases, graphene interlayer hopping (H_{12}) plays a major role in pairing, in contrast to decorated single layer graphene.

In our previous work the possible superconducting phases of lithium decorated single layer graphene LiC_6 were obtained analytically and analyzed.⁹ In that system the Li causes distortion of dominant s -wave and d -wave phases. Due to the existence of a flat band with d -wave Bloch character, d -wave superconducting phases are less affected than are s -wave phases. Generalization of these results to intercalated bilayer graphene is possible through decoupling

of normal and superconducting Hamiltonians of C_6CaC_6 into two independent corresponding single layer pseudo-graphene Hamiltonians, coupled only by a common chemical potential. Similar to the normal state Hamiltonian, the superconducting Hamiltonian is also block diagonalized into two sectors, each similar to single layer pseudo-graphene structures.

As the first result one can see that pairing in bilayer graphene arises between electrons inside of the H_c^+ even sector or H^- odd sectors separately; even-odd pairing is impossible without further symmetry breaking. Two distinct superconductivity gap equations corresponding to H_c^+ and H^- single layer pseudo-graphene structures emerged from minimization of the free energy, which can be considered as the second result. To know whether superconductivity in C_6CaC_6 is single gap or multigap, these two gap equations were solved analytically to obtain the relations between the superconducting pairing potential and resulting ordered phases.

The two sets of gap equations have solutions similar to those obtained for decorated single layer graphene.⁹ There are nine superconducting phases corresponding to each of these gap equations, wherein only three of them are physically reachable, denoted by $\Psi_{\pm,s}^2$, $\Psi_{\pm,dxy}^2$, and $\Psi_{\pm d_{x^2-y^2}}^2$, where the d -wave solutions are degenerate. These three phases are distorted by intercalation i.e. $\alpha_{sy}^{l,\pm} \neq 1$. For the even sector, intralayer pairing amplitudes $\Psi_{\Delta_{sy}}$ and interlayer pairing amplitudes $\Psi'_{\Delta_{sy}}$ are equal, while for odd sector the relation between inter- and intra-layer pairings is $\Psi_{\Delta_{sy}} = -\Psi'_{\Delta_{sy}}$.

Numerical calculations show that for both gap equations d -wave phases, i.e. $\Psi_{\pm,dxy}^2$ and $\Psi_{\pm d_{x^2-y^2}}^2$, are dominant (smaller g_0 means less interaction energy for pairing) and slightly distorted by intercalation i.e. $\alpha_d^{2,\pm} \approx 1$ while s -wave symmetry i.e. $\Psi_{\pm,s}^2$ require greater energy and are significantly distorted, $\alpha_s^{2,\pm} \neq 1$.

These behaviors show that general aspects of superconductivity in the Li-decorated single layer graphene⁹ and Ca intercalated bilayer graphene are similar, and their behaviors are different primarily in the probability of two gap superconductivity in the bilayer structures. A difference of course is that interlayer interaction becomes a key factor. Mathematical analysis shows that in the limit of strong interlayer hoppings, so that inter- and intra- layer hoppings are the same (up to a minus sign), then bandwidths of the even (odd) sector become completely flat while the bandwidths of the other sector are doubled. In this case superconductivity established in the flat bands sector and an extremely small Cooper pairing potential, g_0 leads to a high temperature superconductivity i.e. $g_0 = k_B T_c$. In this limit all of the possible superconducting phases, i.e. d, p and s -wave symmetries, are degenerate.

Although T_c experimentally around 4K and theoretically calculated near 6K are reported, from Fig. 5 it can be seen that both even and odd d -wave phases are nearly degenerate at 2K, consistent with this system being a two gap superconductor around $T_c \approx 2K$. Our results support two gap superconductivity that has been proposed in Ref.[8] (Fig. 2), although different sectors were not separated in their studies.

VII. ACKNOWLEDGMENTS

R. Gholami acknowledges support that allowed an extended visit to the University of California Davis during part of this work. W.E.P. was supported by NSF grant DMR-1207622.

VIII. APPENDIX A: ACCURATE TIGHT BINDING MODEL

In our previous work we used realistic multiband tight binding model for decorated monolayer graphene and obtained its band structure analytically.⁹ Here we follow and generalize that method and find analytic solutions for the intercalated bilayer graphene spectrum in general form. We consider Bloch ket state of Eq.2 as

$$|\Psi_{\vec{k}}(\vec{r})\rangle = \frac{1}{\sqrt{N}} \sum_{n=1}^N \sum_{\alpha=0}^{12} \mathcal{C}_{\alpha} e^{i\vec{k} \cdot \vec{r}_{n\alpha}} |\phi_{n\alpha}\rangle \quad (26)$$

in which $\vec{r}_{n\alpha} = \vec{r}_n + \vec{d}_{\alpha}$ and \vec{r}_n is n th Bravais lattice site vector position and \vec{d}_{α} is vector position of the α -th subsite with respect to unit cell n . The Ca sublattice is labeled by $\alpha = 0$ also $A_1^1, A_2^1, A_3^1, B_1^1, B_2^1, B_3^1, A_1^2, A_2^2, A_3^2, B_1^2, B_2^2, B_3^2$ subsites are labeled by $\alpha = 1, \dots, 12$ respectively. $|\phi_{n\alpha}\rangle = |\phi_{n\alpha}(\vec{r} - \vec{r}_n - \vec{d}_{\alpha})\rangle$ is the atomic π electron ket state of subsite α of site n . The Schrödinger equation for this system is

$$\sum_{\beta=0}^{12} \varepsilon_{\alpha\beta}(\vec{k}) \mathcal{C}_{\beta} + (\varepsilon_{\alpha} - \mu_0) \mathcal{C}_{\alpha} = E(\vec{k}) \mathcal{C}_{\alpha} \quad \text{where} \quad \varepsilon_{\alpha\beta}(\vec{k}) = -\frac{1}{N} \sum_{ij} e^{i\vec{k} \cdot (\vec{r}_{i\alpha} - \vec{r}_{j\beta})} t_{i\alpha j\beta}^{\sigma\sigma}. \quad (27)$$

Symmetries of this system imply that $\mathcal{C}_\alpha(\vec{k}) = \pm \mathcal{C}_{\alpha+6}(\vec{k})$. The Schrödinger equation Eq.27 can be written in the following 13×13 matrix form eigenvalue problem

$$H_N(\vec{k})\Psi_N(\vec{k}) = \begin{bmatrix} h_0(\vec{k}) & h_{01}(\vec{k}) & h_{02}(\vec{k}) \\ h_{10}(\vec{k}) & H_{11}(\vec{k}) & H_{12}(\vec{k}) \\ h_{20}(\vec{k}) & H_{21}(\vec{k}) & H_{22}(\vec{k}) \end{bmatrix} \begin{pmatrix} \mathcal{C}_0(\vec{k}) \\ \mathbf{C}(\vec{k}) \\ \pm \mathbf{C}(\vec{k}) \end{pmatrix} = E_\pm(\vec{k}) \begin{pmatrix} \mathcal{C}_0(\vec{k}) \\ \mathbf{C}(\vec{k}) \\ \pm \mathbf{C}(\vec{k}) \end{pmatrix} \quad (28)$$

where the column matrix $\mathbf{C}(\vec{k})$ is $\mathbf{C}(\vec{k}) = (\mathcal{C}_1(\vec{k}) \mathcal{C}_2(\vec{k}) \dots \mathcal{C}_6(\vec{k}))^T$ and the dispersion matrices satisfy $H_{11} = H_{22}$, $H_{12} = H_{21}$ and $h_{01} = h_{02} = h_{10}^\dagger = h_{20}^\dagger$. The Ca-C dispersion row matrices $h_{01}(\vec{k}) = h_{02}(\vec{k}) = (h_{CaA}(\vec{k}) \ h_{CaB}(\vec{k}))$ are given by

$$\begin{aligned} h_{CaA}(\vec{k}) &= (\varepsilon_{CaA_1}(\vec{k}) \ \varepsilon_{CaA_2}(\vec{k}) \ \varepsilon_{CaA_3}(\vec{k})) = -t_1^{CaC} \begin{pmatrix} e^{i\vec{k} \cdot \vec{\delta}_1} & e^{i\vec{k} \cdot \vec{\delta}_3} & e^{i\vec{k} \cdot \vec{\delta}_2} \end{pmatrix} \\ h_{CaB}(\vec{k}) &= (\varepsilon_{CaB_1}(\vec{k}) \ \varepsilon_{CaB_2}(\vec{k}) \ \varepsilon_{CaB_3}(\vec{k})) = -t_1^{CaC} \begin{pmatrix} e^{-i\vec{k} \cdot \vec{\delta}_1} & e^{-i\vec{k} \cdot \vec{\delta}_3} & e^{-i\vec{k} \cdot \vec{\delta}_2} \end{pmatrix}. \end{aligned} \quad (29)$$

Here t_i^{CaC} is the hopping amplitude from Ca to i th neighbor C atom. The Ca-Ca dispersion is $h_0(\vec{k}) = \varepsilon_{CaCa}(\vec{k}) + \varepsilon_{Ca} - \mu_0$ where

$$\begin{aligned} \varepsilon_{CaCa}(\vec{k}) &= 2t_1^{CaCa} (\cos \vec{k} \cdot \vec{\xi}_1 + \cos \vec{k} \cdot \vec{\xi}_2 + \cos \vec{k} \cdot \vec{\xi}_3) + 2t_2^{CaCa} (\cos \vec{k} \cdot (\vec{\xi}_1 - \vec{\xi}_2) + \cos \vec{k} \cdot (\vec{\xi}_1 - \vec{\xi}_3) + \cos \vec{k} \cdot (\vec{\xi}_2 - \vec{\xi}_3)) \\ &+ 2t_3^{CaCa} (\cos 2\vec{k} \cdot \vec{\xi}_1 + \cos 2\vec{k} \cdot \vec{\xi}_2 + \cos 2\vec{k} \cdot \vec{\xi}_3) + \dots \end{aligned} \quad (30)$$

The interlayer dispersion matrices H_{11} , H_{22} and interlayer dispersion matrices H_{12} and H_{21} are given by

$$H_{mn}(\vec{k}) = \begin{pmatrix} h_{AA}^{mn}(\vec{k}) + (\varepsilon_A^m - \mu_0)\delta_{mn}I_{3 \times 3} & h_{AB}^{mn}(\vec{k}) \\ h_{BA}^{mn}(\vec{k}) & h_{BB}^{mn}(\vec{k}) + (\varepsilon_B^m - \mu_0)\delta_{mn}I_{3 \times 3} \end{pmatrix} \quad (31)$$

where the off-diagonal carbon-carbon dispersion matrices are

$$h_{AA}^{mn}(\vec{k}) = h_{BB}^{*mn}(\vec{k}) = \begin{pmatrix} \varepsilon_{A_1^m A_1^n}(\vec{k}) & \varepsilon_{A_1^m A_2^n}(\vec{k}) & \varepsilon_{A_1^m A_3^n}(\vec{k}) \\ \varepsilon_{A_2^m A_1^n}(\vec{k}) & \varepsilon_{A_2^m A_2^n}(\vec{k}) & \varepsilon_{A_2^m A_3^n}(\vec{k}) \\ \varepsilon_{A_3^m A_1^n}(\vec{k}) & \varepsilon_{A_3^m A_2^n}(\vec{k}) & \varepsilon_{A_3^m A_3^n}(\vec{k}) \end{pmatrix} = \begin{pmatrix} \alpha^{mn}(\vec{k}) & \beta^{mn}(\vec{k}) & \gamma^{mn}(\vec{k}) \\ \beta^{*mn}(\vec{k}) & \alpha^{mn}(\vec{k}) & \theta^{mn}(\vec{k}) \\ \gamma^{*mn}(\vec{k}) & \theta^{*mn}(\vec{k}) & \alpha^{mn}(\vec{k}) \end{pmatrix} \quad (32)$$

$$h_{AB}^{mn}(\vec{k}) = h_{BA}^{\dagger mn}(\vec{k}) = \begin{pmatrix} \varepsilon_{A_1^m B_1^n}(\vec{k}) & \varepsilon_{A_1^m B_2^n}(\vec{k}) & \varepsilon_{A_1^m B_3^n}(\vec{k}) \\ \varepsilon_{A_2^m B_1^n}(\vec{k}) & \varepsilon_{A_2^m B_2^n}(\vec{k}) & \varepsilon_{A_2^m B_3^n}(\vec{k}) \\ \varepsilon_{A_3^m B_1^n}(\vec{k}) & \varepsilon_{A_3^m B_2^n}(\vec{k}) & \varepsilon_{A_3^m B_3^n}(\vec{k}) \end{pmatrix} = \begin{pmatrix} \tau_1^{mn}(\vec{k}) & d_2^{mn}(\vec{k}) & d_3^{mn}(\vec{k}) \\ d_2^{mn}(\vec{k}) & \tau_3^{mn}(\vec{k}) & d_1^{mn}(\vec{k}) \\ d_3^{mn}(\vec{k}) & d_1^{mn}(\vec{k}) & \tau_1^{mn}(\vec{k}) \end{pmatrix} \quad (33)$$

in which m and n are layer index. Shorthand notation has been introduced as follows:

$$\begin{aligned} \beta^{mn}(\vec{k}) &= \varepsilon_{A_1^m A_2^n}(\vec{k}) = \varepsilon_{A_2^m A_1^n}^*(\vec{k}) = t_2^{mn} e^{i\vec{k} \cdot (\vec{\delta}_3 - \vec{\delta}_1)} \left[1 + w_t \left(e^{-i\vec{k} \cdot \vec{\xi}_3} + e^{i\vec{k} \cdot \vec{\xi}_1} \right) \right] \\ \gamma^{mn}(\vec{k}) &= \varepsilon_{A_1^m A_3^n}(\vec{k}) = \varepsilon_{A_3^m A_1^n}^*(\vec{k}) = t_2^{mn} e^{i\vec{k} \cdot (\vec{\delta}_2 - \vec{\delta}_1)} \left[1 + w_t \left(e^{-i\vec{k} \cdot \vec{\xi}_2} + e^{i\vec{k} \cdot \vec{\xi}_1} \right) \right] \\ \theta^{mn}(\vec{k}) &= \varepsilon_{A_2^m A_3^n}(\vec{k}) = \varepsilon_{A_3^m A_2^n}^*(\vec{k}) = t_2^{mn} e^{i\vec{k} \cdot (\vec{\delta}_2 - \vec{\delta}_3)} \left[1 + w_t \left(e^{-i\vec{k} \cdot \vec{\xi}_2} + e^{i\vec{k} \cdot \vec{\xi}_3} \right) \right] \\ \alpha^{mn}(\vec{k}) &= \varepsilon_{A_i^m A_i^n}(\vec{k}) = \varepsilon_{B_i^m B_i^n}(\vec{k}) = t_0^{mn} + 2t_5^{mn} (\cos \vec{k} \cdot \vec{\xi}_1 + \cos \vec{k} \cdot \vec{\xi}_2 + \cos \vec{k} \cdot \vec{\xi}_3) \end{aligned} \quad (34)$$

and it has been supposed that $w_t = \frac{t_1^{mn}}{t_1^{mn}} = \frac{t_2^{mn}}{t_2^{mn}} = \dots$ and $\vec{\xi}_i = \vec{\tau}_i + 2\vec{\delta}_i$. The τ and d -functions are given by

$$\begin{aligned} \tau_1^{mn}(\vec{k}) &= e^{i\vec{k} \cdot \vec{\tau}_1} \left[t_1^{mn} + t_3^{mn} e^{-i\vec{k} \cdot \vec{\xi}_1} + t_4^{mn} \left(e^{i\vec{k} \cdot \vec{\xi}_2} + e^{i\vec{k} \cdot \vec{\xi}_3} \right) \right]; d_1^{mn}(\vec{k}) = e^{i\vec{k} \cdot \vec{\delta}_1} \left[t_1^{mn} + t_3^{mn} e^{-i\vec{k} \cdot \vec{\xi}_1} + t_4^{mn} \left(e^{i\vec{k} \cdot \vec{\xi}_2} + e^{i\vec{k} \cdot \vec{\xi}_3} \right) \right] \\ \tau_2^{mn}(\vec{k}) &= e^{i\vec{k} \cdot \vec{\tau}_2} \left[t_1^{mn} + t_3^{mn} e^{-i\vec{k} \cdot \vec{\xi}_2} + t_4^{mn} \left(e^{i\vec{k} \cdot \vec{\xi}_3} + e^{i\vec{k} \cdot \vec{\xi}_1} \right) \right]; d_2^{mn}(\vec{k}) = e^{i\vec{k} \cdot \vec{\delta}_2} \left[t_1^{mn} + t_3^{mn} e^{-i\vec{k} \cdot \vec{\xi}_2} + t_4^{mn} \left(e^{i\vec{k} \cdot \vec{\xi}_3} + e^{i\vec{k} \cdot \vec{\xi}_1} \right) \right] \\ \tau_3^{mn}(\vec{k}) &= e^{i\vec{k} \cdot \vec{\tau}_3} \left[t_1^{mn} + t_3^{mn} e^{-i\vec{k} \cdot \vec{\xi}_3} + t_4^{mn} \left(e^{i\vec{k} \cdot \vec{\xi}_1} + e^{i\vec{k} \cdot \vec{\xi}_2} \right) \right]; d_3^{mn}(\vec{k}) = e^{i\vec{k} \cdot \vec{\delta}_3} \left[t_1^{mn} + t_3^{mn} e^{-i\vec{k} \cdot \vec{\xi}_3} + t_4^{mn} \left(e^{i\vec{k} \cdot \vec{\xi}_1} + e^{i\vec{k} \cdot \vec{\xi}_2} \right) \right] \end{aligned} \quad (35)$$

Using the following unitary transformation one can separate the bilayer graphene Hamiltonian Eq. 28 into two decoupled single layer pseudo-graphene Hamiltonians, where one of them is decorated with the intercalant layer

$$H_D = Q_T^\dagger H_N(\vec{k}) Q_T = \left[\begin{array}{cc|c} h_0(\vec{k}) & \sqrt{2}h_{01}(\vec{k}) & 0 \\ \sqrt{2}h_{10}(\vec{k}) & H^+(\vec{k}) & 0 \\ \hline 0 & 0 & H^-(\vec{k}) \end{array} \right], \quad Q_T = \frac{1}{\sqrt{2}} \left(\begin{array}{c|cc} \sqrt{2} & 0 & 0 \\ \hline 0 & I_{6 \times 6} & I_{6 \times 6} \\ 0 & I_{6 \times 6} & -I_{6 \times 6} \end{array} \right). \quad (36)$$

Here $H^\pm = H_{11}(\vec{k}) \pm H_{12}$ in matrix notation is

$$H^\pm(\vec{k}) = H_{11}(\vec{k}) \pm H_{12}(\vec{k}) = \left(\begin{array}{ccc|ccc} \varepsilon_1^\pm(\vec{k}) & \beta^\pm(\vec{k}) & \gamma^\pm(\vec{k}) & \tau_1^\pm(\vec{k}) & d_2^\pm(\vec{k}) & d_3^\pm(\vec{k}) \\ \beta^{\pm*}(\vec{k}) & \varepsilon_1^\pm(\vec{k}) & \theta^\pm(\vec{k}) & d_2^\pm(\vec{k}) & \tau_3^\pm(\vec{k}) & d_1^\pm(\vec{k}) \\ \gamma^{\pm*}(\vec{k}) & \theta^{\pm*}(\vec{k}) & \varepsilon_1^\pm(\vec{k}) & d_3^\pm(\vec{k}) & d_1^\pm(\vec{k}) & \tau_2^\pm(\vec{k}) \\ \hline \tau_1^{\pm*}(\vec{k}) & d_2^{\pm*}(\vec{k}) & d_3^{\pm*}(\vec{k}) & \varepsilon_2^\pm(\vec{k}) & \beta^{\pm*}(\vec{k}) & \gamma^{*\pm}(\vec{k}) \\ d_2^{\pm*}(\vec{k}) & \tau_3^{\pm*}(\vec{k}) & d_1^{\pm*}(\vec{k}) & \beta^\pm(\vec{k}) & \varepsilon_2^\pm(\vec{k}) & \theta^{\pm*}(\vec{k}) \\ d_3^{\pm*}(\vec{k}) & d_1^{\pm*}(\vec{k}) & \tau_2^{\pm*}(\vec{k}) & \gamma^\pm(\vec{k}) & \theta^\pm(\vec{k}) & \varepsilon_2^\pm(\vec{k}) \end{array} \right) \quad (37)$$

in which \vec{k} -dependent on-site energies have been defined as $\varepsilon_1^\pm(\vec{k}) = \varepsilon_A - \mu_0 + \alpha^\pm(\vec{k})$ and $\varepsilon_2^\pm(\vec{k}) = \varepsilon_B - \mu_0 + \alpha^\pm(\vec{k})$. Also the following shorthand notation has been introduced

$$\begin{aligned} \alpha^\pm(\vec{k}) &= \left(\alpha^{11}(\vec{k}) \pm \alpha^{12}(\vec{k}) \right), \quad \beta^\pm(\vec{k}) = \left(\beta^{11}(\vec{k}) \pm \beta^{12}(\vec{k}) \right); \quad \tau_i^\pm(\vec{k}) = \left(\tau_i^{11}(\vec{k}) \pm \tau_i^{12}(\vec{k}) \right) \\ \gamma^\pm(\vec{k}) &= \left(\gamma^{11}(\vec{k}) \pm \gamma^{12}(\vec{k}) \right), \quad \theta^\pm(\vec{k}) = \left(\theta^{11}(\vec{k}) \pm \theta^{12}(\vec{k}) \right); \quad d_i^\pm(\vec{k}) = \left(d_i^{11}(\vec{k}) \pm d_i^{12}(\vec{k}) \right) \end{aligned} \quad (38)$$

Unitary transformation of Eq. 36 divides **thirteen** bands of intercalated bilayer graphene into, **six** and **seven** bands groups. Following the approach⁹ that has been applied to monolayer decorated graphene, an exact analytical solution of the six-band group can be found in general case. These bands are eigenvalues of H^- matrix and are not affected directly by the intercalant band.

In the special case of pristine bilayer graphene in which $\gamma^{\pm*}(\vec{k}) = \theta^\pm(\vec{k}) = \beta^\pm(\vec{k})$, $\varepsilon_1^\pm(\vec{k}) = \varepsilon_2^\pm(\vec{k})$ and $\tau_i^\pm(\vec{k}) = d_i^\pm(\vec{k})$, Eq. 37 easily can be diagonalized to find eigenvalues and also eigenvectors. The eigenvalues are given by

$$E_{\gamma,l}^\pm = \varepsilon_1^\pm(\vec{k}) + \beta^\pm(\vec{k}) + \beta^{*\pm}(\vec{k}) + (-1)^l t_1^\pm |\eta_0^\pm(\vec{k})| \quad (39)$$

$$E_{\alpha,l}^\pm = \varepsilon_1^\pm(\vec{k}) + e^{i2\pi/3} \beta^\pm(\vec{k}) + e^{-i2\pi/3} \beta^{*\pm}(\vec{k}) + (-1)^l t_1^\pm |\eta_1^\pm(\vec{k})| \quad (40)$$

$$E_{\beta,l}^\pm = \varepsilon_1^\pm(\vec{k}) + e^{-i2\pi/3} \beta^\pm(\vec{k}) + e^{i2\pi/3} \beta^{*\pm}(\vec{k}) + (-1)^l t_1^\pm |\eta_2^\pm(\vec{k})| \quad (41)$$

with eigenvectors are given by replacing m in the following equation with $m = 0, 1, 2$ respectively

$$\phi_{m,l}^\pm(\vec{k}) = \frac{1}{\sqrt{6}} [(u_m \quad u_m^* \quad 1) \quad (-1)^l \frac{\eta_m^{*\pm}}{|\eta_m^\pm|} (u_m^* \quad u_m \quad 1)]^T \quad (42)$$

wherein

$$\eta_m^\pm(\vec{k}) = d_2^\pm(\vec{k}) + u_m d_1^\pm(\vec{k}) + u_m^* d_3^\pm(\vec{k}); \quad u_m = e^{i2m\pi/3} \quad (43)$$

However, except at Γ point it is challenging (and unhelpful) to obtain an exact forms of the seven-band group analytically. These bands are eigenvalues of the H_c^+ matrix, and analytic expressions for them can be obtained just in the particular case of no hopping between intercalant layer and graphene sheet, similar to the case for lithium intercalated bilayer graphene where intercalant band is empty (no Li-C hopping). In these cases nontrivial solutions are eigenvalues of H^+ matrix. Eigenvalues of H^- and H^+ matrices are given by⁹

$$E_{sh,m,l}^\pm(t_i, \vec{\xi}_i, \vec{k}) = \mu_m^\pm(\vec{k}) - \mu_0 + \frac{1}{2} \left[\varepsilon_A + \varepsilon_B + (-1)^l \sqrt{(\varepsilon_A - \varepsilon_B)^2 + 4w_m^\pm(t_i, \vec{\xi}_i, \vec{k})} \right], \quad m = 1, 2, 3; \quad l = 1, 2 \quad (44)$$

in which \vec{k} dependent chemical potentials are defined as,

$$\mu_m^\pm(\vec{k}) = \alpha^\pm(\vec{k}) + u_m \Pi_0^\pm(t_2, \vec{\xi}_i, \vec{k}) + u_m^* \Pi_0^{\pm*}(t_2, \vec{\xi}_i, \vec{k}); \quad u_m = e^{2im\pi/3}. \quad (45)$$

The $\Pi_0^\pm(t_2, \vec{\xi}_i, \vec{k})$ function is introduced as

$$\Pi_0^\pm(t_2, \vec{\xi}_i, \vec{k}) = \left(\frac{c_0^\pm(t_2, \vec{\xi}_i, \vec{k})}{2} + i\sqrt{\left(\frac{c_1^\pm(t_2, \vec{\xi}_i, \vec{k})}{3}\right)^3 - \left(\frac{c_0^\pm(t_2, \vec{\xi}_i, \vec{k})}{2}\right)^2} \right)^{1/3}. \quad (46)$$

and, $c_0^\pm(t_2, \vec{\xi}_i, \vec{k}) = \gamma^{\pm*}(\vec{k})[\beta^\pm(\vec{k})\theta^\pm(\vec{k})] + \gamma^\pm(\vec{k})[\beta^{\pm*}(\vec{k})\theta^{\pm*}(\vec{k})]^*$ and $c_1^\pm(t_2, \vec{\xi}_i, \vec{k}) = |\beta^\pm(\vec{k})|^2 + |\theta^\pm(\vec{k})|^2 + |\gamma^\pm(\vec{k})|^2$. Also, $w_m^\pm(t_i, \vec{\xi}_i, \vec{k})$ are eigenvalues of the following matrices

$$G^\pm = \begin{pmatrix} \tau_1^\pm(\vec{k}) & d_2^\pm(\vec{k}) & d_3^\pm(\vec{k}) \\ d_2^\pm(\vec{k}) & \tau_3^\pm(\vec{k}) & d_1^\pm(\vec{k}) \\ d_3^\pm(\vec{k}) & d_1^\pm(\vec{k}) & \tau_1^\pm(\vec{k}) \end{pmatrix} \begin{pmatrix} \tau_1^{\pm*}(\vec{k}) & d_2^{\pm*}(\vec{k}) & d_3^{\pm*}(\vec{k}) \\ d_2^{\pm*}(\vec{k}) & \tau_3^{\pm*}(\vec{k}) & d_1^{\pm*}(\vec{k}) \\ d_3^{\pm*}(\vec{k}) & d_1^{\pm*}(\vec{k}) & \tau_1^{\pm*}(\vec{k}) \end{pmatrix}. \quad (47)$$

The eigenvalues can be obtained as

$$w_m^\pm(t_i, \vec{\xi}_i, \vec{k}) = \frac{C_2^\pm(t_i, \vec{\xi}_i, \vec{k})}{3} + u_m \Pi_1^\pm(t_i, \vec{\xi}_i, \vec{k}) + u_m^* \Pi_1^{\pm*}(t_i, \vec{\xi}_i, \vec{k}), \quad u_m = e^{2im\pi/3}; \quad m = 1, 2, 3. \quad (48)$$

wherein

$$\begin{aligned} C_2^\pm(t_i, \vec{\xi}_i, \vec{k}) &= G_{11}^\pm + G_{22}^\pm + G_{33}^\pm \\ C_1^\pm(t_i, \vec{\xi}_i, \vec{k}) &= |G_{12}^\pm|^2 + |G_{13}^\pm|^2 + |G_{23}^\pm|^2 - (G_{11}^\pm G_{22}^\pm + G_{11}^\pm G_{33}^\pm + G_{22}^\pm G_{33}^\pm) \\ C_0^\pm(t_i, \vec{\xi}_i, \vec{k}) &= G_{13}^\pm (G_{12}^\pm G_{23}^\pm)^* + G_{13}^{\pm*} (G_{12}^\pm G_{23}^\pm) - G_{11}^\pm |G_{23}^\pm|^2 - G_{22}^\pm |G_{13}^\pm|^2 - G_{33}^\pm |G_{12}^\pm|^2 + G_{11}^\pm G_{22}^\pm G_{33}^\pm \end{aligned} \quad (49)$$

$$\begin{aligned} \Pi_1^\pm(t_i, \vec{\xi}_i, \vec{k}) &= \left(Q^\pm(t_i, \vec{\xi}_i, \vec{k}) + i\sqrt{P^\pm(t_i, \vec{\xi}_i, \vec{k})^3 - Q^\pm(t_i, \vec{\xi}_i, \vec{k})^2} \right)^{\frac{1}{3}} \\ Q^\pm(t_i, \vec{\xi}_i, \vec{k}) &= \frac{C_0^\pm(t_i, \vec{\xi}_i, \vec{k})}{2} + \frac{C_1^\pm(t_i, \vec{\xi}_i, \vec{k})C_2^\pm(t_i, \vec{\xi}_i, \vec{k})}{6} + \frac{C_2^{\pm 3}(t_i, \vec{\xi}_i, \vec{k})}{27} \\ P^\pm(t_i, \vec{\xi}_i, \vec{k}) &= \frac{C_1^\pm(t_i, \vec{\xi}_i, \vec{k})}{3} + \frac{C_2^{\pm 2}(t_i, \vec{\xi}_i, \vec{k})}{9}. \end{aligned} \quad (50)$$

One can write the H_D matrix in H^\pm bases i. e. $H'_D = U^\dagger H_D U$,

$$H'_D = \begin{pmatrix} h_0(\vec{k}) & \gamma_1(\vec{k}) & \gamma_2(\vec{k}) & \gamma_3(\vec{k}) & \gamma_4(\vec{k}) & \gamma_5(\vec{k}) & \gamma_6(\vec{k}) & 0 & 0 & 0 & 0 & 0 & 0 \\ \gamma_1^*(\vec{k}) & E_1^+(\vec{k}) & 0 & 0 & 0 & 0 & 0 & 0 & 0 & 0 & 0 & 0 & 0 \\ \gamma_2^*(\vec{k}) & 0 & E_2^+(\vec{k}) & 0 & 0 & 0 & 0 & 0 & 0 & 0 & 0 & 0 & 0 \\ \gamma_3^*(\vec{k}) & 0 & 0 & E_3^+(\vec{k}) & 0 & 0 & 0 & 0 & 0 & 0 & 0 & 0 & 0 \\ \gamma_4^*(\vec{k}) & 0 & 0 & 0 & E_4^+(\vec{k}) & 0 & 0 & 0 & 0 & 0 & 0 & 0 & 0 \\ \gamma_5^*(\vec{k}) & 0 & 0 & 0 & 0 & E_5^+(\vec{k}) & 0 & 0 & 0 & 0 & 0 & 0 & 0 \\ \gamma_6^*(\vec{k}) & 0 & 0 & 0 & 0 & 0 & E_6^+(\vec{k}) & 0 & 0 & 0 & 0 & 0 & 0 \\ \hline 0 & 0 & 0 & 0 & 0 & 0 & 0 & E_1^-(\vec{k}) & 0 & 0 & 0 & 0 & 0 \\ 0 & 0 & 0 & 0 & 0 & 0 & 0 & 0 & E_2^-(\vec{k}) & 0 & 0 & 0 & 0 \\ 0 & 0 & 0 & 0 & 0 & 0 & 0 & 0 & 0 & E_3^-(\vec{k}) & 0 & 0 & 0 \\ 0 & 0 & 0 & 0 & 0 & 0 & 0 & 0 & 0 & 0 & E_4^-(\vec{k}) & 0 & 0 \\ 0 & 0 & 0 & 0 & 0 & 0 & 0 & 0 & 0 & 0 & 0 & E_5^-(\vec{k}) & 0 \\ 0 & 0 & 0 & 0 & 0 & 0 & 0 & 0 & 0 & 0 & 0 & 0 & E_6^-(\vec{k}) \end{pmatrix} \quad (51)$$

The upper left portion of Eq.51 can be obtained sufficiently well by perturbation theory.

IX. APPENDIX B: BOGOLIUBOV-DE GENNES TRANSFORMATION

The interacting Hamiltonian H_{su} in matrix representation is 14×14 matrix,

$$H_{su}(\vec{k}) = \sum_{\vec{k}} \hat{\Psi}^\dagger(\vec{k}) \begin{pmatrix} H_N(\vec{k}) & H_P(\vec{k}) \\ H_P^\dagger(\vec{k}) & -H_N^*(-\vec{k}) \end{pmatrix} \hat{\Psi}(\vec{k}) \quad (52)$$

where $\hat{\Psi}^\dagger(\vec{k}) = (\hat{c}_{0\uparrow}^\dagger(\vec{k})\hat{c}_{1\uparrow}^\dagger(\vec{k})\hat{c}_{2\uparrow}^\dagger(\vec{k}) \dots; \hat{c}_{12\uparrow}^\dagger(\vec{k})\hat{c}_{0\downarrow}(-\vec{k})\hat{c}_{1\downarrow}(-\vec{k})\hat{c}_{2\downarrow}(-\vec{k}) \dots \hat{c}_{12\downarrow}(-\vec{k}))$. H_N is Hamiltonian of the normal state and H_p is the pair interaction matrix. The full matrix must be diagonalized to obtain the quasiparticle spectrum.

The mean field superconducting Hamiltonian of Eq. 1 in Nambu space is $\hat{H}_{su} = \sum_{\vec{k}} \hat{\Psi}^\dagger(\vec{k})H_{su}(\vec{k})\hat{\Psi}(\vec{k})$ where H_{su} in matrix representation is,

$$H_{su}(\vec{k}) = \begin{pmatrix} H_N(\vec{k}) & H_P(\vec{k}) \\ H_P^\dagger(\vec{k}) & -H_N^*(-\vec{k}) \end{pmatrix} = \begin{pmatrix} \left(\begin{array}{c|cc} h_0(\vec{k}) & h_{01}(\vec{k}) & h_{02}(\vec{k}) \\ \hline h_{10}(\vec{k}) & H_{11}(\vec{k}) & H_{12}(\vec{k}) \\ h_{20}(\vec{k}) & H_{21}(\vec{k}) & H_{22}(\vec{k}) \end{array} \right) & \begin{bmatrix} 0 & 0 & 0 \\ 0 & H_{11}^P(\vec{k}) & H_{12}^P(\vec{k}) \\ 0 & H_{21}^P(\vec{k}) & H_{22}^P(\vec{k}) \end{bmatrix} \\ \left[\begin{array}{c|cc} 0 & 0 & 0 \\ \hline 0 & H_{11}^P(\vec{k}) & H_{12}^P(\vec{k}) \\ 0 & H_{21}^P(\vec{k}) & H_{22}^P(\vec{k}) \end{array} \right] & - \begin{pmatrix} h_0(\vec{k}) & h_{01}(\vec{k}) & h_{02}(\vec{k}) \\ \hline h_{10}(\vec{k}) & H_{11}(\vec{k}) & H_{12}(\vec{k}) \\ h_{20}(\vec{k}) & H_{21}(\vec{k}) & H_{22}(\vec{k}) \end{pmatrix} \end{pmatrix} \quad (53)$$

and $\hat{\Psi}^\dagger(\vec{k}) = (\hat{c}_{0\uparrow}^\dagger(\vec{k})\hat{c}_{1\uparrow}^\dagger(\vec{k})\hat{c}_{2\uparrow}^\dagger(\vec{k}) \dots; \hat{c}_{12\uparrow}^\dagger(\vec{k})\hat{c}_{0\downarrow}(-\vec{k})\hat{c}_{1\downarrow}(-\vec{k})\hat{c}_{2\downarrow}(-\vec{k}) \dots \hat{c}_{12\downarrow}(-\vec{k}))$ where $H_{11}(\vec{k}) = H_{22}(\vec{k})$. The interlayer pairing matrices are $H_{11}^P(\vec{k}) = H_{22}^P(\vec{k})$ and interlayer pairing matrices are $H_{12}^P(\vec{k}) = H_{21}^P(\vec{k})$. The pairing matrices are given by

$$H_{mn}^P(\vec{k}) = \begin{pmatrix} \begin{array}{ccc|ccc} 0 & 0 & 0 & \Sigma_1^{mn}(\vec{k}) & \Delta_2^{mn}(\vec{k}) & \Pi_3^{mn}(\vec{k}) \\ 0 & 0 & 0 & \Pi_2^{mn}(\vec{k}) & \Sigma_3^{mn}(\vec{k}) & \Delta_1^{mn}(\vec{k}) \\ 0 & 0 & 0 & \Delta_3^{mn}(\vec{k}) & \Pi_1^{mn}(\vec{k}) & \Sigma_2^{mn}(\vec{k}) \\ \hline \Sigma_1^{mn*}(\vec{k}) & \Pi_2^*(\vec{k}) & \Delta_3^{mn*}(\vec{k}) & 0 & 0 & 0 \\ \Delta_2^{mn*}(\vec{k}) & \Sigma_3^{mn*}(\vec{k}) & \Pi_1^{mn*}(\vec{k}) & 0 & 0 & 0 \\ \Pi_3^{mn*}(\vec{k}) & \Delta_1^{mn*}(\vec{k}) & \Sigma_2^{mn*}(\vec{k}) & 0 & 0 & 0 \end{array} \end{pmatrix} \quad (54)$$

where m and n are layer index which can take 1 or 2. The order parameters accordingly in Fourier space are

$$\begin{aligned} \Sigma_l^{11}(\vec{k}) &= g_1 \Sigma_{l<ij>} e^{i\vec{k}\cdot\vec{\tau}_i}, & \Sigma_l^{12}(\vec{k}) &= g'_1 \Sigma'_{l<ij>} e^{i\vec{k}\cdot\vec{\tau}_i} \\ \Pi_l^{11}(\vec{k}) &= g_0 \Pi_{l<ij>} e^{i\vec{k}\cdot\vec{\delta}_i}, & \Pi_l^{12}(\vec{k}) &= g'_0 \Pi'_{l<ij>} e^{i\vec{k}\cdot\vec{\delta}_i} \\ \Delta_l^{11}(\vec{k}) &= g_0 \Delta_{l<ij>} e^{i\vec{k}\cdot\vec{\delta}_i}, & \Delta_l^{12}(\vec{k}) &= g'_0 \Delta'_{l<ij>} e^{i\vec{k}\cdot\vec{\delta}_i}, \quad l = 1, 2, 3. \end{aligned} \quad (55)$$

where $<ij>$ subscript indicate nearest neighbor pairing amplitude in real space as illustrated in Fig.1. Introducing the following unitary transformation matrix,

$$\hat{H}_{su} = \sum_{\vec{k}} \hat{\Psi}^\dagger(\vec{k})Q \left[Q^\dagger H_{su}(\vec{k})Q \right] Q \hat{\Psi}(\vec{k}) = \sum_{\vec{k}} \Lambda^\dagger(\vec{k})H_s(\vec{k})\Lambda(\vec{k}), \quad Q = \begin{pmatrix} Q_T(\vec{k}) & 0 \\ 0 & \hat{Q}_T^*(-\vec{k}) \end{pmatrix}, \quad (56)$$

one can transform Eq.56. Eq.53 can be transformed to the block diagonalize form

$$\hat{H}_{su} = \sum_{\vec{k}} \Lambda^\dagger(\vec{k}) \begin{pmatrix} H_{su}^+(\vec{k}) & 0 \\ 0 & H_{su}^-(\vec{k}) \end{pmatrix} \Lambda(\vec{k}) \quad (57)$$

in which

$$H_{su}^+(\vec{k}) = \begin{pmatrix} H_c^+(\vec{k}) & H_p^+(\vec{k}) \\ H_p^+(\vec{k}) & -H_c^+(\vec{k}) \end{pmatrix}_{14 \times 14}, \quad H_{su}^-(\vec{k}) = \begin{pmatrix} H^-(\vec{k}) & H_p^-(\vec{k}) \\ H_p^-(\vec{k}) & -H^-(\vec{k}) \end{pmatrix}_{12 \times 12} \quad (58)$$

and, $\Lambda^\dagger(\vec{k}) = \left([\hat{c}_{0\uparrow}^\dagger(\vec{k})\hat{c}_{1\uparrow}^\dagger(\vec{k})\dots\hat{c}_{6\uparrow}^\dagger(\vec{k})\hat{c}_{0\downarrow}(-\vec{k})\hat{c}_{1\downarrow}(-\vec{k})\dots\hat{c}_{6\downarrow}(-\vec{k})] \quad [\hat{c}_{1\uparrow}^\dagger(\vec{k})\hat{c}_{2\uparrow}^\dagger(\vec{k})\dots\hat{c}_{6\uparrow}^\dagger(\vec{k})\hat{c}_{1\downarrow}(-\vec{k})\hat{c}_{2\downarrow}(-\vec{k})\dots\hat{c}_{6\downarrow}(-\vec{k})] \right)$, where $\hat{c}_{m\sigma}^{(\pm)\dagger}(\vec{k}) = \frac{1}{\sqrt{2}}(\hat{c}_{m\sigma}^\dagger(\vec{k}) \pm \hat{c}_{m+6,\sigma}^\dagger(\vec{k}))$. New pairing matrices $H_p^+(\vec{k})$ and $H_p^-(\vec{k})$ are defined as,

$$H_p^+(\vec{k}) = \begin{pmatrix} 0 & 0 \\ 0 & H_p^{11}(\vec{k}) + H_p^{12}(\vec{k}) \end{pmatrix}, \quad H_p^-(\vec{k}) = \begin{pmatrix} H_p^{11}(\vec{k}) - H_p^{12}(\vec{k}) \end{pmatrix}. \quad (59)$$

From Eq. 57 it can be seen that the superconducting Hamiltonian H_{su} can be diagonalized into two decoupled new superconducting Hamiltonian H_{su}^+ and H_{su}^- . Thus electrons just can be paired within the seven band sector H_c^+ or within the six bands sector H^- , without coupling between the sectors. Thus superconductivity in bilayer graphene can be interpreted as two decoupled monolayer graphene-like systems with independent behaviors.

X. APPENDIX C: TWO SUPERCONDUCTING GAP EQUATIONS

The linearized superconducting gap equation are obtained by minimizing the quasiparticle free energy with respect to the nearest neighbor order parameter, or equivalently with respect to Δ_{\pm}^{α} . The free energy of system is

$$F = F^+ + F^- + F_0 = -\frac{2}{\beta} \sum_{\vec{k}} \sum_{n=1}^{13} \ln \left[2 \cosh \left(\frac{E_n^Q}{2k_B T} \right) \right] + F_0, \quad F_0 = -2N \sum_{\alpha=1}^{18} J_{\alpha} (\Delta^{\alpha})^2. \quad (60)$$

For F^+ the summation runs over $n = 1, \dots, 7$ giving $E_n^Q = E_{n,s}^{Q+}$; for F^- the summation takes $n = 8, \dots, 13$ values giving $E_n^Q = E_{n,s}^{Q-}$, with $E_{n,s}^{Q\pm}$ introduced in Eqs. 12 and 13.

Minimization of the free energy with respect to Δ_{\pm}^{α} gives

$$\Delta_{\langle ij \rangle}^{\beta} + \Delta'_{\langle ij \rangle}{}^{\beta} = -\frac{1}{N} \sum_{\alpha=1}^9 \left[\sum_{\vec{k}} \sum_{n=1}^7 \sum_{i=1}^7 \frac{\tanh \left(\frac{E_n^{Q+}}{2k_B T} \right)}{E_n^+(\vec{k}) + E_i^+(\vec{k})} \left(\Omega_{ni}^{+\alpha}(\vec{k}) \Omega_{ni}^{+\beta}(\vec{k}) + \Omega_{ni}^{+\beta}(\vec{k}) \Omega_{ni}^{+\alpha}(\vec{k}) \right) \right] \Delta_{\pm}^{\alpha} \equiv -\sum_{\alpha=1}^9 \Gamma_{\beta\alpha}^+ \Delta_{\pm}^{\alpha}. \quad (61)$$

giving independent gap equations for the seven band odd-symmetry graphene-like Hamiltonian H_c^+ . Minimizing the free energy with respect to Δ_{\pm}^{α} gives

$$\Delta_{\langle ij \rangle}^{\beta} - \Delta'_{\langle ij \rangle}{}^{\beta} = -\frac{1}{N} \sum_{\alpha=1}^9 \left[\sum_{\vec{k}} \sum_{n=1}^6 \sum_{i=1}^6 \frac{\tanh \left(\frac{E_n^{Q-}}{2k_B T} \right)}{E_n^-(\vec{k}) + E_i^-(\vec{k})} \left(\Omega_{ni}^{-\alpha}(\vec{k}) \Omega_{ni}^{-\beta}(\vec{k}) + \Omega_{ni}^{-\beta}(\vec{k}) \Omega_{ni}^{-\alpha}(\vec{k}) \right) \right] \Delta_{\pm}^{\alpha} \equiv -\sum_{\alpha=1}^9 \Gamma_{\beta\alpha}^- \Delta_{\pm}^{\alpha}. \quad (62)$$

where Δ^{α} as illustrated in Fig.1(b) covers all possible nearest neighbor inter- and intra-layer C-C pairing amplitudes. Eqs. 61 and Eq. 62 in matrix form written as

$$\begin{bmatrix} A^{\pm} & B^{\pm} & B^{\pm} \\ B^{\pm} & C^{\pm} & D^{\pm} \\ B^{\pm} & D^{\pm} & C^{\pm} \end{bmatrix} \begin{pmatrix} g_1 \Sigma_i \pm g'_1 \Sigma'_i \\ g_0 \Pi_i \pm g'_0 \Pi'_i \\ g_0 \Delta_i \pm g'_0 \Delta'_i \end{pmatrix} = - \begin{pmatrix} \Sigma_i \pm \Sigma'_i \\ \Pi_i \pm \Pi'_i \\ \Delta_i \pm \Delta'_i \end{pmatrix}. \quad (63)$$

Equivalently, Eqs. 61 and 62 can be combined in the following non-Hermitian eigenvalue problem,

$$\begin{bmatrix} G^+ & \kappa_0 G^- \\ G^- & \kappa_0 G^+ \end{bmatrix} \begin{pmatrix} \Psi_{\Delta} \\ \Psi'_{\Delta} \end{pmatrix} = -\frac{1}{g_0} \begin{pmatrix} \Psi_{\Delta} \\ \Psi'_{\Delta} \end{pmatrix} \quad (64)$$

in which $\kappa_0 = \frac{g_0}{g'_0}$ and

$$G^{\pm} = \frac{1}{2} \begin{bmatrix} \kappa(A^+ \pm A^-) & \kappa(B^+ \pm B^-) & \kappa(B^+ \pm B^-) \\ (B^+ \pm B^-) & (C^+ \pm C^-) & (D^+ \pm D^-) \\ (B^+ \pm B^-) & (D^+ \pm D^-) & (C^+ \pm C^-) \end{bmatrix}, \quad \Psi_{\Delta} = \begin{pmatrix} g_1 V_1 \\ g_0 V_2 \\ g_0 V_3 \end{pmatrix}, \quad \Psi'_{\Delta} = \begin{pmatrix} g'_1 V'_1 \\ g'_0 V'_2 \\ g'_0 V'_3 \end{pmatrix}. \quad (65)$$

$\kappa = \frac{g_1}{g'_0} = \frac{g'_1}{g_0}$, $V_1^T = (\Sigma_1 \ \Sigma_2 \ \Sigma_3)$, $V_2^T = (\Pi_1 \ \Pi_2 \ \Pi_3)$, and $V_3^T = (\Delta_1 \ \Delta_2 \ \Delta_3)$. Also $V_1'^T = (\Sigma'_1 \ \Sigma'_2 \ \Sigma'_3)$, $V_2'^T = (\Pi'_1 \ \Pi'_2 \ \Pi'_3)$, and $V_3'^T = (\Delta'_1 \ \Delta'_2 \ \Delta'_3)$. Equation 64 is in fact the matrix representation of gap equation resulting from minimization of the free energy with respect to nearest neighbor order parameters instead of Δ_{\pm}^{α} , which can be solved to obtain the differing superconductivity phases and pairing interaction potentials.

In the limiting case $\kappa_0 \rightarrow 1$, the inter- and intra-layer pairing amplitudes in real space are equal, *i.e.* $g_0 = g'_0$ and $g_1 = g'_1$. This restriction makes the matrix gap equation hermitian and implies that band order parameters $\Delta_{mn}^{\pm}(\vec{k})$ can be interpreted physically as pairing of electrons in different bands with pairing interaction g_0^{\pm} . Just in this limit $\Delta_{mn}^{\pm}(\vec{k})$ is equal to the product of band Green function and g_0 ,

$$\Delta_{mn}^{\pm}(\vec{k}) = g_0^{\pm} \langle \hat{d}_m^{\pm\uparrow}(\vec{k}) \hat{d}_n^{\pm\downarrow}(\vec{k}) \rangle. \quad (66)$$

Here $\hat{d}_i^{\pm\sigma}(\vec{k}) = \sum_{m=1}^7 \mathcal{C}_m^{\pm*}(E_i(\vec{k})) \hat{c}_m^{\sigma}(\vec{k})$ annihilates an electron with spin σ in the i th six (odd) or seven (even) sector bands with energy $E_i^{\pm}(\vec{k})$. In this limit, Eq. 64 has two solutions $\Psi_{\Delta} = \Psi'_{\Delta}$ or $\Psi_{\Delta} = -\Psi'_{\Delta}$. The corresponding gap equations Eqs. 63 and 64 become decoupled gap equations corresponding to the even or odd sector of the graphene-like systems.

$$F^+ \Psi_{\Delta} = g_0^+ \Psi_{\Delta}, \quad F^- \Psi_{\Delta} = g_0^- \Psi_{\Delta}, \quad F^{\pm} = \begin{bmatrix} A^{\pm} & B^{\pm} & B^{\pm} \\ B^{\pm} & C^{\pm} & D^{\pm} \\ B^{\pm} & D^{\pm} & C^{\pm} \end{bmatrix} \quad (67)$$

XI. APPENDIX D: FLAT BAND(S) SUPERCONDUCTIVITY

Mirror symmetry transformation rearranges the noninteracting Hamiltonian Eq. 2 as the direct sum of two single layer pseudo-graphene structures $\hat{H}_N = \hat{H}_N^+ \oplus \hat{H}_N^-$ (even sector (+ sign) and odd sector (- sign))

$$\hat{H}_N^+ = \sum_{ij\sigma} \sum_{\alpha,\beta=0}^6 t_{i\alpha\sigma,j\beta\sigma}^+ \hat{c}_{i\alpha\sigma}^{+\dagger} \hat{c}_{j\beta\sigma}^+; \quad \hat{H}_N^- = \sum_{ij\sigma} \sum_{\alpha,\beta=1}^6 t_{i\alpha\sigma,j\beta\sigma}^- \hat{c}_{i\alpha\sigma}^{-\dagger} \hat{c}_{j\beta\sigma}^- \quad (68)$$

with renormalized hopping integrals of the form $t_{i\alpha\sigma,j\beta\sigma}^{\pm} = t_{i\alpha\sigma,j\beta\sigma}^{inter} \pm t_{i\alpha\sigma,j\beta+6\sigma}^{intra}$. In the limit case of strong interlayer hopping wherein $t_{i\alpha\sigma,j\beta\sigma}^{inter} \rightarrow \pm t_{i\alpha\sigma,j\beta+6\sigma}^{intra}$ one can see that odd (or even) sector bandwidths completely become flat while the other sector bandwidth doubles. In this limit, thermal weight factor of Eq. 18 $\frac{\tanh(\frac{\beta E_i^{\pm}}{2})}{E_j^{\pm}(\vec{k}) + E_i^{\pm}(\vec{k})} \rightarrow \frac{\beta}{4}$ and so Γ matrix elements are given by

$$\Gamma_{\beta\alpha}^{\pm} = \frac{\beta}{4N} \sum_{\vec{k}} \sum_{ij} \left(\Omega_{ij}^{\pm\alpha}(\vec{k}) \Omega_{ji}^{\pm\beta}(\vec{k}) + \Omega_{ji}^{\pm\alpha}(\vec{k}) \Omega_{ij}^{\pm\beta}(\vec{k}) \right). \quad (69)$$

These elements are linked to the normal state Bloch coefficients via the $\Omega_{ij}^{\pm\beta}(\vec{k})$ factors that given by Eq. 14. For the case of pristine bilayer graphene, Eq. 69 can be determined analytically. In this limit, normal state Bloch coefficients are given by

$$[\mathcal{C}_1^{\pm}(E_{ml}) \dots \mathcal{C}_6^{\pm}(E_{ml})] = \frac{1}{\sqrt{6}} [(u_m \quad u_m^* \quad 1) \quad (-1)^l e^{i\phi_m^{\pm}(\vec{k})} (u_m^* \quad u_m \quad 1)]; \quad u_m = e^{i2m\pi/3}, \quad m = 1, 2, 3 \quad \& \quad l = 1, 2 \quad (70)$$

wherein $e^{i\phi_m^{\pm}(\vec{k})} = \frac{u_m^*}{|\eta_m^{\pm}|}$ and $\eta_m^{\pm}(\vec{k}) = d_2^{\pm}(\vec{k}) + u_m d_1^{\pm}(\vec{k}) + u_m^* d_3^{\pm}(\vec{k})$. $\Omega_{ij}^{\pm\beta}(\vec{k})$ factors can be calculated by substituting Bloch coefficients Eq. 70 in the Eq. 14. For instant one can show

$$\begin{aligned} \Omega_{11}^{\pm 1}(\vec{k}) &= \Omega_{11}^{\pm 4}(\vec{k}) = \Omega_{11}^{\pm 7}(\vec{k}) = -\frac{1}{3} \cos(\vec{k} \cdot \vec{\delta}_1 - \phi_1^{\pm}(\vec{k})) \\ \Omega_{11}^{\pm 2}(\vec{k}) &= \Omega_{11}^{\pm 5}(\vec{k}) = \Omega_{11}^{\pm 8}(\vec{k}) = -\frac{1}{3} \cos(\vec{k} \cdot \vec{\delta}_2 - \phi_1^{\pm}(\vec{k})) \\ \Omega_{11}^{\pm 3}(\vec{k}) &= \Omega_{11}^{\pm 6}(\vec{k}) = \Omega_{11}^{\pm 9}(\vec{k}) = -\frac{1}{3} \cos(\vec{k} \cdot \vec{\delta}_3 - \phi_1^{\pm}(\vec{k})) \\ \Omega_{16}^{\pm 1}(\vec{k}) &= \Omega_{16}^{\pm 4}(\vec{k}) = \Omega_{16}^{\pm 7}(\vec{k}) = -\frac{i}{3} \sin(\vec{k} \cdot \vec{\delta}_1 - \phi_1^{\pm}(\vec{k})) \\ \Omega_{16}^{\pm 2}(\vec{k}) &= \Omega_{16}^{\pm 5}(\vec{k}) = \Omega_{16}^{\pm 8}(\vec{k}) = -\frac{i}{3} \sin(\vec{k} \cdot \vec{\delta}_2 - \phi_1^{\pm}(\vec{k})) \\ \Omega_{16}^{\pm 3}(\vec{k}) &= \Omega_{16}^{\pm 6}(\vec{k}) = \Omega_{16}^{\pm 9}(\vec{k}) = -\frac{i}{3} \sin(\vec{k} \cdot \vec{\delta}_3 - \phi_1^{\pm}(\vec{k})) \end{aligned} \quad (71)$$

By calculating a large number of these factors and replacing them in the Eq. 69 one can obtain

$$\Gamma_{ij}^{\pm} = \beta_c \delta_{ij}; \quad g_0 = k_B T_c$$

XII. REFERENCES

* Electronic address: rmoradian@razi.ac.ir

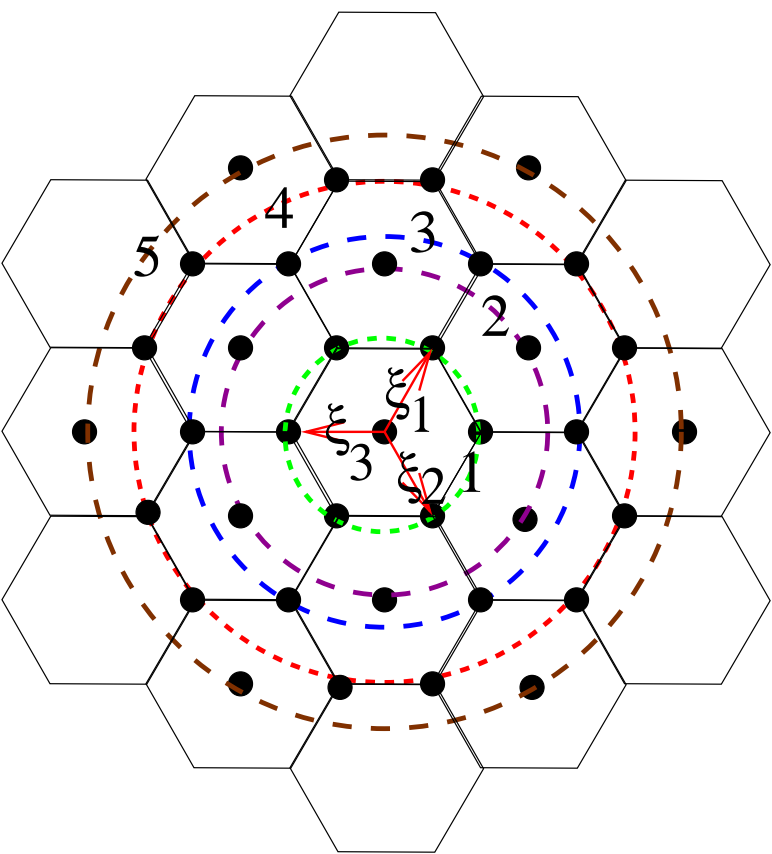
¹ C. Brun, T. Cren, and D. Roditchev, Review of 2D superconductivity: the ultimate case of epitaxial monolayers, *Supercond. Sci. & Technol.* **30**, 013003 (2017).

² T. E. Weller *et al.*, Superconductivity in the intercalated graphite compounds C₆Yb and C₆Ca, *Nat. Phys.* **1**, 39 (2005).

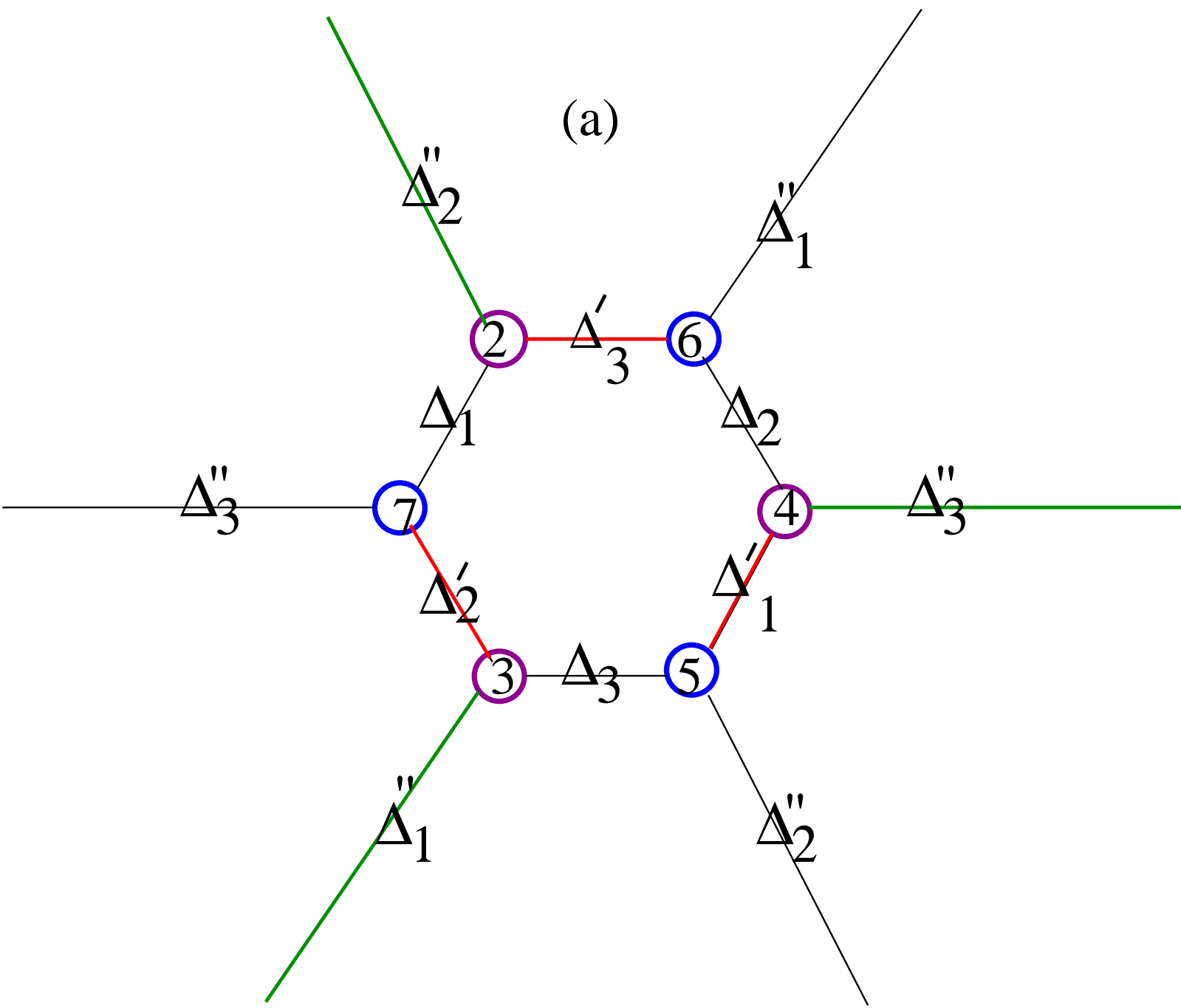
³ Y. Cao, V. Fatemi, S. Fang, K. Watanabe, T. Taniguchi, E. Kaxiras, and P. Jarillo-Herrero, Unconventional superconductivity in magic-angle graphene superlattices, *Nature* **556**, 43 (2018). doi:10.1038/nature26160.

- ⁴ S. Ichinokura *et al.*, Superconducting calcium-intercalated bilayer graphene, ACS Nano **10**, 2761 (2016).
- ⁵ J. Chapman *et al.*, Superconductivity in Ca-doped graphene laminates, Sci. Rep. **6**, 23254 (2016).
- ⁶ B.M. Ludbrook *et al.*, Evidence for superconductivity in Li-decorated monolayer graphene, Proc. Natl. Acad. Sci. (USA) **112**, 11795-11799 (2015).
- ⁷ A. P. Tiwari, S. Shin, D. Hwang, S. G. Jung, T. Park, and H. Lee, Superconductivity at 7.4K in few layer graphene by Li intercalation, J. Phys.: Condens. Matt. **29**, 445701 (2017).
- ⁸ E. R. Margine, H. Lambert, and F. Giustino, Electron-phonon interaction and pairing mechanism in superconducting Ca-intercalated bilayer graphene, Sci. Rep. **6**, 21414 (2016).
- ⁹ R. Gholami, R. Moradian, S. Moradian, W. E. Pickett, Superconducting phases of lithium intercalated graphene, Sci. Rep. **8**, 13795 (2018). doi: 10.1038/s41598-018-32050-9.
- ¹⁰ J. Vucicevic, M. O. Goerbig, and M. V. Milovanovic, *d*-wave superconductivity on the honeycomb bilayer, Phys. Rev. B **86**, 214505 (2012).
- ¹¹ J. M. Murray and O. Vafek, Excitonic and superconducting orders from repulsive interaction on the doped honeycomb bilayer, Phys. Rev. B **89**, 205119 (2014).

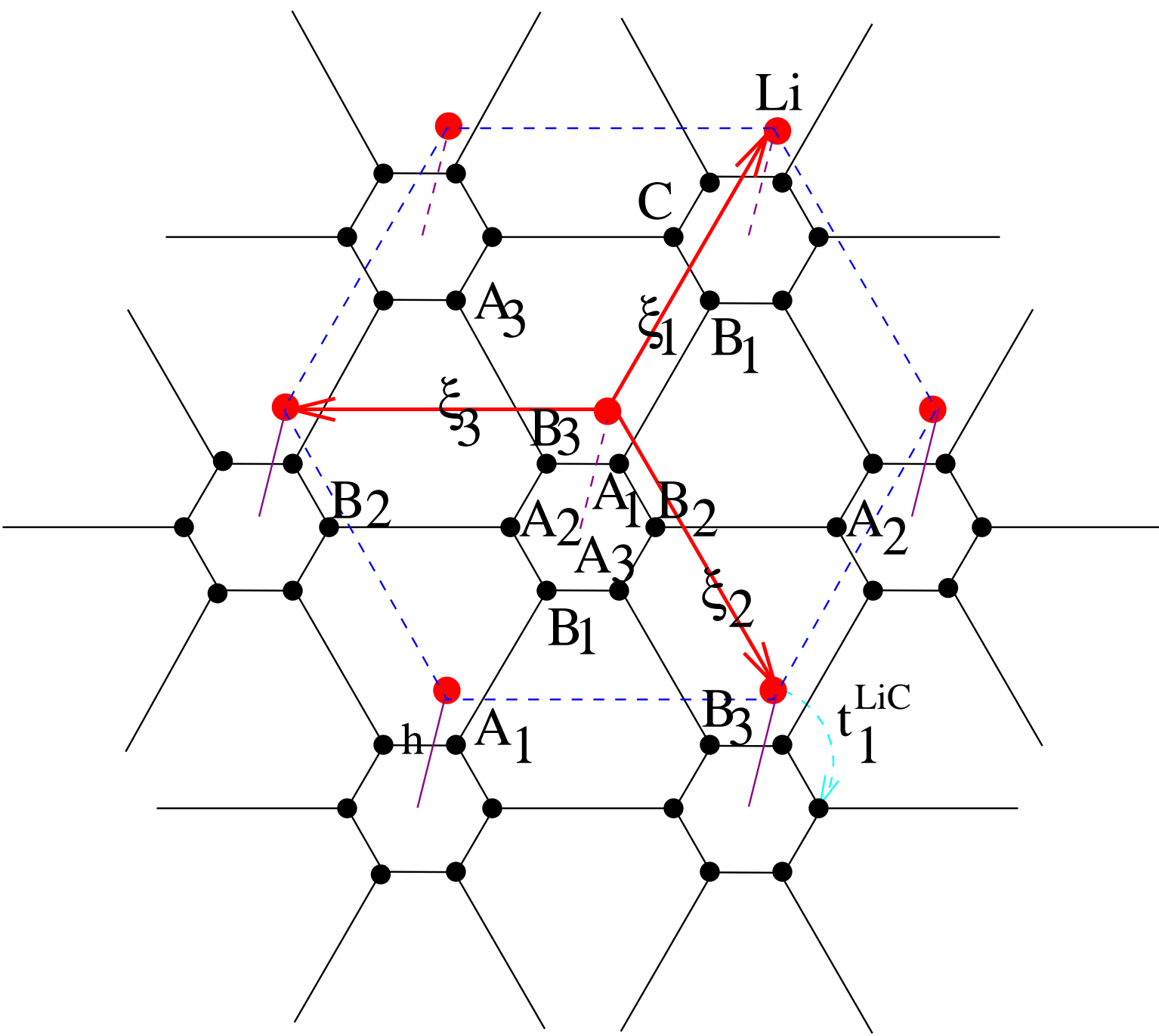
(b)



(a)



(c)



(a)

